[1]Gilbert Langat, Beiji Zou

[1]Xiaoyan Kui

[1]Kevin Njagi

An Efficient Multiple Sclerosis Segmentation Framework using Hybrid Dilated Convolution –based Adaptive Mobilenet Mechanism.

Journal of Electrical Systems

Abstract: - Multiple Sclerosis (MS) is considered a very popular neurological condition in adults. Poor walking stability is considered the primary sign of MS. The Magnetic Resonance Imaging (MRI) is ensured to be a delicate approach for discovering disease progression. Severity quantification of the disease via MS lesion volume validation with MR imaging is significant for monitoring and learning the disorder and its treatment. Numerous techniques for MS lesions segmentation demand experts seed points as input, yet do not sufficiently permit the specialists to perform effectively or intuitively. Interestingly, various approaches also consider that the points are optimally determined. Hence, it is necessary to rectify some of the troubles that existed in classical MS classification mechanisms by developing a powerful process with deep learning in this work. In the beginning, the requisite MS images are fetched from the existing online source and forwarded to the module of image segmentation. In this module, an efficient image segmentation operation is carried out employing Transformer Unet++ with MobileNetv3 (TUnet++-MNetv3). Further, the segmented images are given to the module named MS classification, where the Hybrid Dilated Convolution based Adaptive MobileNet (HDC-AMNet) is recommended to classify the MS. Moreover, the Enhanced Single Candidate Optimizer (ESCO) is adopted to optimize the parameters that exist in the MobileNet. Thus, the designed MS classification task achieves improved performance rates by contrasting it with its baseline techniques employing numerous metrics.

Keywords: Multiple Sclerosis Classification; Abnormality Segmentation; Transformer Unet++ with MobileNetv3; Hybrid Dilated Convolution based Adaptive MobileNet; Enhanced Single Candidate Optimizer

I. INTRODUCTION

MS is referred to as a general inflammatory neurological situation troubling the central nervous system. It leads to degeneration of axonal and demyelization mostly in the brain's white matter [9]. The symptoms highly change from individual to individual, with general symptoms such as visual impairment, fatigue, depression, balance issues, and weakness [10]. Based on the inflammation location named plaques diverse symptoms grow. These plaques may be diagnosed by the MRI but not Computed Tomography (CT). The MRI is considered an effective component for monitoring the disease progression and is also employed for diagnosing the disease [11]. The medical experts employ 'Fluid-Attenuated Inversion Recovery (FLAIR), T1-weighted (T1-w), and T2-weighted (T2-w)' sequences to detect the axonal damage and inflammatory lesions yet sensitivity based on the slice thickness and are time-consuming and laborious [12]. The FLAIR, T1-w, and T2-w are considered distinct pulse series of the MRI that are achieved by distinct relaxation periods. Computerized segmentation and identification models can win over these problems [13]. Though decades of research focus, the cognitive variations encountered in people with various MS start to be one of the most obstinate symptoms [14]. The manual segmentation task's subjective nature, time consumption, explaining ground truth lesion data, variation in intra-expert and inter-expert, and the MRI data's heterogeneous intensity have made it complex to develop an effective segmentation approach for identifying and quantifying the lesions of MS [15]. Hence, the automatic identification and segmentation of the lesions in MS have become a significant problem for follow-up and diagnosis in clinical practice.

Numerous automated MS lesion identification mechanisms have been implemented over these years [16]. Experts have conducted an automated approach according to the volume subtraction, and intensity normalization in the MR images to recognize the lesions of MS. Most of these mechanisms are according to the machine learning techniques and data mining hence demanding more training to draw out the MS regions to several extent [17]. Examples of these approaches are 'Genetic Algorithm (GA), Support Vector Machine (SVM), clustering, and Artificial Neural Network (ANN)'. An automatic approach for detecting MS is to favor knowledge exploring mechanisms including clustering for evaluation of healthcare images [18]. Moreover, for simplicity, these

[1] School of Computer Science, Central South University, 410083, China

Corresponding Author: gilbert langat email: gilbertmarisa161@hotmail.com

Copyright © JES 2024 on-line : journal.esrgroups.org

mechanisms are effective for the analysis of healthcare images. These conventional mechanisms offer successive outcomes, however, these techniques require to extract the features previously [19]. Normally, the experts can grasp numerous features. But, it is complex to explain the representative attributes. Thus, the selection and integration of features become a significant complexity for the developers [20].

Because of the changes in dimension, region, and shape among people, identification of the MS lesions in MRI is highly complex [21]. The MRI is an important early detection of high-risk individuals. Based on this fact, it has been employed in the sector of MS disease research [22]. The necessary developments have been conducted for the segmentation using conventional machine learning approaches and in the past decades, deep learning mechanisms made specific improvements in the recognition, detection, and segmentation operations [23]. Some of the techniques have been explained for the automatic identification and segmentation of MS lesions in MRI. In the current days, some of the Convolutional NNs (CNNs) and other techniques have been recommended to diagnose MS lesions automatically because of their promising functionality contrasted with traditional approaches [24]. However, these techniques faced some disadvantages. For instance, several techniques demand pre-processing like segmentation and several techniques demand pre-processing to enhance the classification that results in computational burden [25]. In addition to that, most of the mechanisms have issues like blurring that have not been addressed. Hence, developing an effective MS classification model is significant.

The designed classification framework for MS consists of below contributions.

- To construct a novel approach for classifying the MS by utilizing improved optimization-assisted deep learning with abnormality segmentation that supports the radiologists to make decisions timely to cure the individual.

- To perform the abnormality segmentation by adopting a new TUnet++-MNetv3 technique which is the integration of transUnet++ and MoboleNetV3 approaches. This TUnet++-MNetv3 technique segments the abnormalities even if the region is too small.

- To design an effective ESCO algorithm with the assistance of traditional SCO for optimizing the parameters and improving the system convergence rates. Moreover, this ESCO also helps to enhance the precision and accuracy rates and minimizes error rates.

- To build a new technique named HDC-AMNet, which is the integration of hybrid dilated convolution and MobileNet for classifying the MS. Here, the recommended ESCO is utilized for optimizing MobileNet's parameters.

- To verify and contrast the implemented classification framework by employing traditional techniques and algorithms. This proves the robustness and efficacy of the developed classification model.

The layout of the designed MS classification framework is given as follows. Part II illustrates the existing classification techniques for MS. Part III describes an automated system of MS classification: dataset and recommended model description. Part IV portrays the abnormality segmentation utilizing TUnet++-MNetv3. Part V elucidates the HDC-AMNet for classifying the MS. Part VI shows a detailed description of the experiments. Part VII gives the conclusion of the suggested work.

II. EXISTING WORKS

A. Related Works

In 2020, Ye *et al.* [1] integrated Diffusion Basis Spectrum Imaging (DBSI) with the Deep NN (DNN) and other imaging techniques to address the heterogeneity of MS lesions. The DBSI-DNN enhanced the classification of distinct MS lesions sub-categories. The efficacy of the DBSI-DNN displayed better outcomes for the medical systems in the automatic classification of MS lesions.

In 2020, Wang *et al.* [2] have suggested an advanced transfer learning-assisted mechanism. Here, a pre-computation task was employed to minimize the storage complexity and enhance the process. The experts contrasted the developed model with other traditional techniques. Experts monitored that the model attained the best functionality.

In 2020, Soltani *et al.* [3] have introduced a CNN-assisted approach to diagnose the MS lesions from MRI. The recommended task minimized the network parameters usage and relatively enhanced the learning speed. The CNN offered good outcomes without a requirement for lesions segmentation and also gave a very low sensitivity rate to the complexities of distinct contrasts and blurring. The developed task offered better accuracy and specificity.

In 2021, Martin *et al.* [4] diagnosed the initial stages of MS patients according to the evaluation of retinal layer thickness achieved with the assistance of Optical Coherence Tomography (OCT). The presented work employed the feed-forward NN and SVM. The developed work recommended that the OCT might support a significant part of other clinical experiments most importantly concerning Neuro-degeneration.

In 2020, Cetin *et al.* [5] have focussed on implementing a new, simple, and robust image segmentation process to conduct the evaluation of MS lesions from MRI data. This work employed the Euclidean distance-aided clustering approach for 3 MRI modalities including T2w, T1w. The segmentation of distinct brain tissue employing the author's model provided superior outcomes contrasted with the traditional mechanisms.

In 2021, Buyukturkoglu *et al.* [6] recommended an approach to forecast the white matter variations in early MS. This work employed random forests to train the techniques. From the techniques, the features were extracted and fused. The outcomes offered high accuracy and assisted as a powerful Neuro-imaging biomarker in early MS.

In 2021, Iswisi *et al.* [7] employed the Harris Hawks optimization (HHO) model for selecting the cluster centers optimally in the segmentation process. The HHO was more accurate than the other traditional techniques. The suggested HHO minimized the clustering error of the MS. Based on the experiment performed on the number of brain MRIs, the suggested work performed better than the other mechanisms.

In 2021, Afzal *et al.* [8] have presented a fully automated CNN task with 2D pathways. The first CNN was developed to segment the lesions precisely and the second CNN was concentrated to minimize the false positives. Experts determined the implemented work with complex and public data sources. The developed task provided higher sensitivity and precision than the other techniques.

B. Research Gaps and Challenges

The MS is a neurological condition that can affect the patient's nerves. It is recorded as the growing reason for the non-traumatic neurologic disability among adults. The symptoms of this disease are very severe and lead to very little possibility of complete recovery. Hence, experts concentrate on implementing various frameworks to diagnose the MS. However, the traditional MS classification techniques meet the following issues.

∗ Most of the traditional MS classification techniques didn't perform the abnormality segmentation that minimized the efficacy of the conventional techniques. Hence, the implemented MS classification process performed the segmentation task using enhanced techniques.

∗ The conventional MS classification techniques consume more time to perform the parameter tuning. Hence, the recommended MC classification technique employed an improved heuristic approach that quickly discovers the optimal solutions.

∗ The conventional MS classification frameworks are hard to interpret and demand more computational resources. To tackle these issues, the designed work is implemented with advanced deep-learning models.

∗ Developing an automatic MS classification technique with high accuracy is still a primary concern for experts. Hence, this developed work produced a highly accurate MS classification model that assists medical experts in making clear decisions.

∗ The traditional MS classification techniques can't work effectively in huge data sources. Hence, this work developed a framework to work effectively even with huge data sources.

Thus, a brand new MS classification approach is presented in this paper to resolve the mentioned problems. Table 1 offers the merits and complexities faced in several traditional MS classification techniques.

TABLE I. **FEATURES AND CHALLENGES OF EXISTING MS CLASSIFICATION APPROACHES**

Author [citation]	Methodology	Features	Challenges
Ye *et al.* [1]	DNN	• It can make results with high accuracy. • It decreases the complexity of the model.	• Its cost for the computation is high. • It demands more computational resources.
Wang *et al.* [2]	DenseNet-201	• It minimizes the gradient issues. • It enhances feature reuse and feature propagation.	• Its network model is very complex. • It is sensitive to overfitting.
Soltani *et al.* [3]	CNN	• It extracts features without human intervention. • It can capture very complex features effectively.	• It takes more time for training. • It consumes more power for computation.
Martin *et al.* [4]	NN	• It is an automatic and flexible network. • It reduces the dimensionality issues of the images.	• It has high computational burden. • It needs more cost and time.
Cetin *et al.* [5]	Clustering method	• It discovers the hidden and complex features of an image. • It improves the accuracy rates.	• It has poor interpretability. • It is highly susceptible to outliers and noise.
Buyukturkoglu *et al.* [6]	Random forest	• It is very accurate and effective. • It can handle large datasets precisely.	• It is ineffective for real-time applications. • It is too slow due to the high amount of trees.
Iswisi *et al.* [7]	HHO	• It has a strong search capacity. • It utilizes very less parameters.	• It can easily fall into local optimum. • It has premature convergence.
Afzal *et al.* [8]	CNN	• It accurately executes the huge data sources. • It reduces the steps of computation.	• It is a very slow network. • It is prone to overfitting issues.

III. AUTOMATED SYSTEM OF MULTIPLE SCLEROSIS CLASSIFICATION: DATASET AND PROPOSED MODEL DESCRIPTION

A. Illustrative of Suggested Multiple Sclerosis Classification

MS is considered a chronic disorder that affects an individual's central nervous system. In MS, the nervous system is damaged and these damages go away after several weeks if these injuries are not critical, however can cause

constant changes in the nervous system if these injuries are critical. These persistent variations are named sclerosis and due to these lesions in distinct and multiple regions, the disorder is named MS. To detect MS, various screening techniques have been suggested so far; among them, the MRI has attained high attention among medical experts. The modalities of MRI offers offer medical experts with necessary details regarding the function and the structure of the brain that is significant for the timely MS lesion diagnosis. However, diagnosing MS lesions with the assistance of MRI is tedious, tiresome, and susceptible to errors. Experiments on the development of a Computer Aided Diagnosis System (CADS)-aided by Artificial Intelligence (AI) to classify the MS. However, in traditional machine learning, the steps are performed based on trial and error. Moreover, the traditional techniques demand numerous skills in multiple AI sectors. Contrarily, deep learning methodologies are the advanced versions of AI that have gained more popularity. The techniques in deep learning do not demand any manual intervention to extract the feature. However, implementing a more accurate MS classification model utilizing deep learning remains a complex work because of the technique's high resource consumption, computational complexity, and dimensionality issues. Thus, this work implemented a framework for diagnosing MS utilizing deep learning. The deep learning-assisted classification system for MS is displayed in Fig.1.

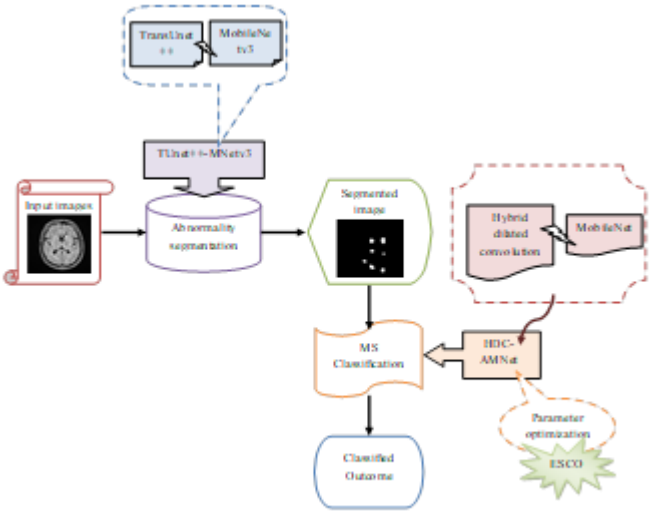

Figure 1 Illustration of deep learning-assisted MS classification framework

The developed classification system of MS is introduced in the work in an advanced way. Initially, the necessary images are fetched from the benchmark data sources for performing the subsequent tasks. The obtained images are further offered to the segmentation operation. This step is carried out by utilizing the TUnet++-MNetv3 technique, which effectively segmented the abnormalities present in the gathered images. The suggested TUnet++-MNetv3 technique is integrated with transformer Unet++ and MobileNetv3. This stage improves the image quality and removes unnecessary outliers. Further, the resultant images are taken to the MS classification module, where the MS lesions are categorized by the HDC-AMNet technique. The mentioned HDC-AMNet technique is the integration of the hybrid dilated convolution and the MobileNet. In addition to that, this stage employs the ESCO technique to optimize the parameters in MobileNet. Hence, the MS classification process achieved high accuracy and precision rates. The experiments were conducted on the implemented classification system of MS lesions to verify the implemented framework's robustness.

B. Image Collection

The images that are necessary for performing the MS classification framework are acquired from the below dataset.

Dataset ("Brain MRI Dataset of Multiple Sclerosis with Consensus Manual Lesion Segmentation and Patient Meta Information"): By using the link "https://data.mendeley.com/datasets/8bctsm8jz7/1: access date: 2023-04-08" this data source is obtained. This resource includes the MRI of 60 sick persons by manual lesions

segmentation, sick person, and medical data. The MRI sequences including FLAIR, T1, and T2 are presented in this data source. With this data source, the relation between the clinical data of patients and MS lesions is determined.

The sample images fetched from this data source are given in Fig.2, and the gathered images are specified as S_c, *here* $c = 1,2,3,..,C$ for further processing. Here, C is the total amount of images.

"Description"	1	2	3	4	5
"FLAIR images"					
"Normal"	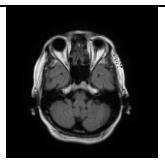	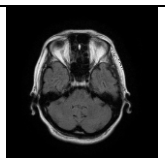	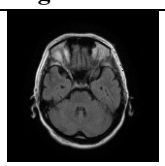	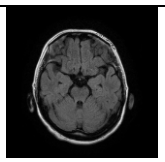	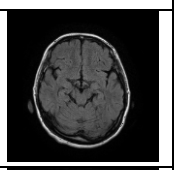
"Abnormal"	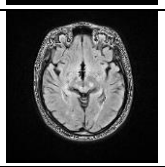	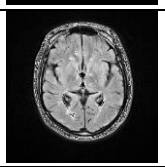	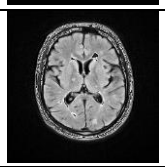	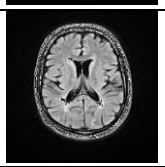	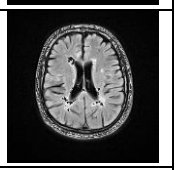
"T1 images"					
"Normal"	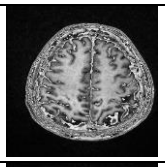	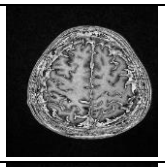	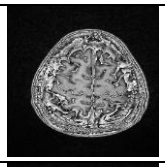	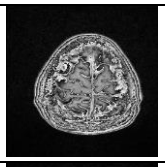	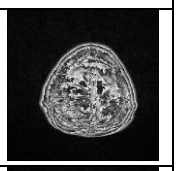
"Abnormal"	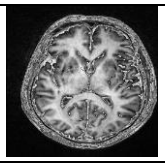	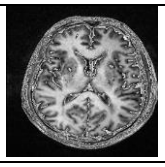	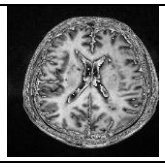		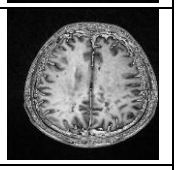
"T2 images"					
"Normal"	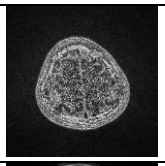	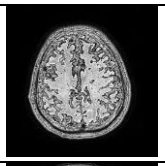	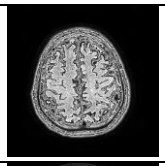	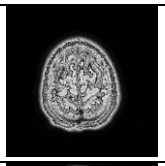	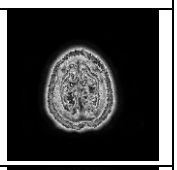
"Abnormal"	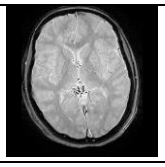	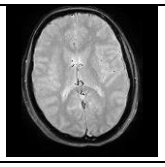	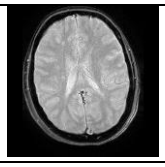	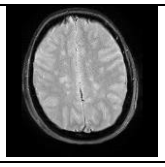	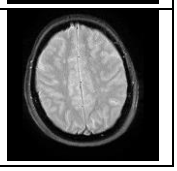

Figure 2 Sample images employed for recommended classification framework of MS

C. Parameter Tuning by ESCO

The recommended ESCO is the improved approach of the existing SCO. This SCO is performed by utilizing the single-member outcome. The recommended ESCO is truly developed for optimizing the parameters of MobileNet in HDC-AMNet technique that increases the precision and accuracy of the approach. Besides, it assists in minimizing the error rates of the process. By employing the ESCO the optimal outcomes are achieved for the developed classification framework for MS. The traditional SCO employs some of the expressions to upgrade the positions of candidates. Unfortunately, the existing SCO employs arbitrary factors in the range of [0, 1] for exploring the solutions. Hence, it results in slow convergence rates. Hence, to resolve this issue, the ESCO is presented in this work by introducing a new random factor p_3. This new random factor p_3 is implemented with the assistance of fitness values and supports to update the position. This improves the convergence rates of the model. In addition to that, it quickly discovers the optimal outcomes. Thus, the ESCO is implemented. The newly determined random variable's p_3 formulation is shown in Eq. (1).

$$p_3 = \frac{bts}{\sqrt{bts^{1.5} + wts^{1.5}}} \quad (1)$$

Here, the worst fitness factor and best fitness factor are declared respectively. By utilizing this formulation (Eq.1), the position of SCO is upgraded in Eq. (5). The significant concepts of conventional SCO are presented as follows.

The conventional SCO [26] is mimicked by the outcome of a single member in the overall process. Here, a two-phase process is conducted to trade off the exploration and exploitation modules. In the two-phase tasks, the first phase performed the γ function estimation, while the second phase performed the λ function estimation, where $\gamma + \lambda = W$. Here, W is the highest iteration.

The candidate's solution updating is expressed in Eq. (2) at the starting stage of SCO.

$$i_l = \begin{cases} hbt_l + (b \mid hbt_l \mid), & if \quad p_1 < 0.5 \\ hbt_l - (b \mid hbt_l \mid), & otherwise \end{cases} \quad (2)$$

The random factor in the limit of 0 and 1 is pointed as p_1 and the factor b is derived in Eq. (3).

$$b(w) = \exp^{-\left(\frac{tw}{W}\right)^s} \quad (3)$$

Here, t is the constant variable, and function evaluation is given as w.

Further, the next stage is performed by updating the position of the candidate as given in Eq. (4).

$$i_l = \begin{cases} hbt_l + (p_2 b \mid m_l - o_l \mid), & if \quad p_2 < 0.5 \\ hbt_l - (p_2 b \mid m_l - o_l \mid), & otherwise \end{cases} \quad (4)$$

This stage employed another random factor p_2 in the range of 0 and 1. Further, the upper and lower regions are provided $o_l \ and \ n_l$.

After this process, if the periodical function estimations do not revise the fitness values, and then based on Eq. (5), the position is updated.

$$i_l = \begin{cases} hbt_l + (p_3 \mid m_l - o_l \mid), & if \quad p_3 < 0.5 \\ hbt_l - (p_3 \mid m_l - o_l \mid), & otherwise \end{cases} \quad (5)$$

In the above derivation also, the traditional SCO employs another arbitrary variable in the limit of 0 and 1. However, this random factor didn't improve the convergence rates while updating the positions. This leads to premature convergence rates for the model. Hence, with the support of Eq. (1), a brand new random integer p_3 is implemented in ESCO that is upgraded in Eq. (5). Hence, the convergence rate of the model is improved and assists in discovering the optimal outcomes. This updated Eq. (5) prevents the local optimum issues.

Upgrading the places of some of the factors in SCO can cause its values to go out of the boundaries. To tackle these, utilizing Eq. (6), the places are upgraded for the candidates.

$$i_l = \begin{cases} hbt_l, & if \quad p_l > m_l \\ hbt_l, & if \quad p_l < o_l \end{cases} \quad (6)$$

In the existing SCO, the solution of a single member is randomly produced and it is upgraded to discover the efficient solution. This is commenced with randomly producing a member solution in the discovering sector, determining its fitness, sealing this member as hbt, and its fitness is considered as $r(hbt)$ the best fitness overall. The initial candidate outcome is given in Eq. (7).

$$i_l = n_l + p_4(m_l - o_l) \tag{7}$$

Algorithm 1 depicts the pseudo-code for developed ESCO and its flowchart is presented in Fig.3.

Algorithm 1: Recommended ESCO

The population and iteration initialization
Fitness function evaluation
For $w=1$ *to* $W_{\max}$
  For $l=1$ *to* N_{pop}
    Utilizing Eq. (1), new arbitrary factor p_3 estimation
    Utilizing Eq. (2), position updating of starting stage
    Second stage position updating employing Eq. (4) and Eq. (5)
    Creation of starting candidate employing Eq. (7)
    Update the better positions

End
End
Conduct the repetitive tasks
Return the achieved outcomes

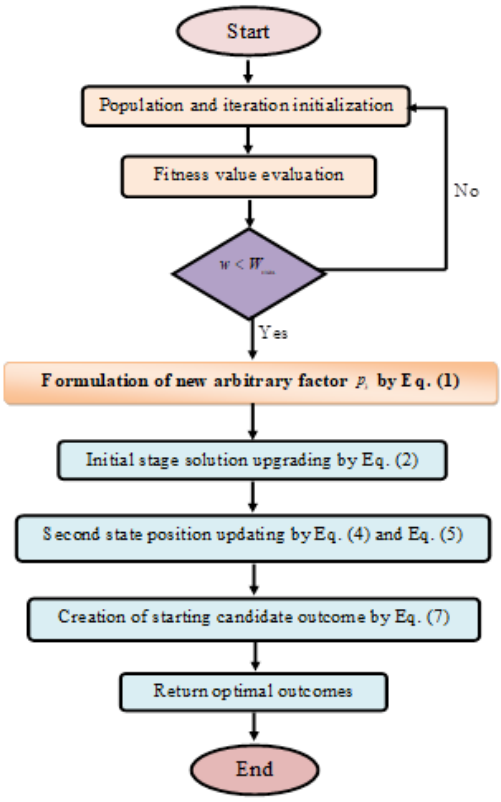

Figure 3 Flowchart of recommended ESCO for optimizing the parameters

IV. ABNORMALITY SEGMENTATION USING TRANSFORMER-BASED UNET++ WITH MOBILENETV3

A. TransUnet++

The transUnet++ is the integration of the transformer and Unet++. The transformer [27] is relatively based on the task named self-attention. It achieved better success in the segmentation tasks. The self-attention process cannot discover the positions, hence in the transformer network, the positional encoding is integrated.

By using the matrix format $I \in \Re^{x,c}$, the transformer encoder is considered where the length of the sequence is pointed as x and the input dimension is given as c. Further, three matrices $M_y, M_u,$ *and* M_w are assisted to enlarge I into distinct spaces. The size of the three matrices is taken as $\Re^{c \times c_u}$, where c_u is the hyper attribute. Eq. (8) to Eq. (10) explains the scaled dot product attention.

$$Y, U, W = IM_y, IM_u, IM_w \tag{8}$$

$$P_{d,f} = A_d U_f^D \tag{9}$$

$$Atn(Y, U, W) = soft\max\left(\frac{P}{\sqrt{c_u}}\right)W \tag{10}$$

Here, the query vector and token attend are indicated as A_d *and* f for the d^{th} token. The key vector is represented as U_f the d^{th} token. Eq. (11) to Eq. (13) formulate the multi-head self-attention.

$$Y^{(i)}, U^{(i)}, I^{(i)} = IM_y^{(i)}, IM_u^{(i)}, IM_w^{(i)} \tag{11}$$

$$head^{(i)} = Atn\left(Y^{(i)}, U^{(i)}, I^{(i)}\right) \tag{12}$$

$$multi - head(I) = \left[head^{(1)}; ...; head^{(q)}\right]M_R \tag{13}$$

The count of heads is noted as q and is a head index. The term $\left[head^{(1)}; ...; head^{(q)}\right]$refers to the fusion in the final dimension.

The solution of the multi-head attention is fed into the position-wise feed-forward network. This is derived in Eq. (14).

$$ffn(s) = \max(0, sM_1 + v_1)M_2 + v_2 \tag{14}$$

Here, the learnable attributes are given as $M_1, M_2, v_1,$ *and* v_2.

In the transformer, the self-attention couldn't discover the distinct token's places. To rectify this issue, the position embedding is produced in the transformer. The position embedding for d^{th} tokens is formulated in Eq. (15) and Eq. (16).

$$pe_{d,2j} = \sin\left(\frac{d}{10000^{\frac{2j}{c}}}\right) \tag{15}$$

$$pe_{d,2j+1} = \cos\left(\frac{d}{10000^{\frac{2j}{c}}}\right) \tag{16}$$

Here, j is in the limit of $\left[0, \frac{c}{2}\right]$.

The UNet++ [28] is the improved category of the UNet. The UNet includes of encoder and decoder that is in the shape of a U. This is highly employed to train upon several data samples. Generally, the UNet framework is the 23-layered framework including ReLU and reprocessed unpadded convolutions. For the downsampling, the UNet includes maxpooling. It also contains the modules such as a decoder, skip connections, bridge, and encoder. When considering UNet++, the semantic void among the decoder and encoder modules is incorporated by the existence of convolutional layers with skip connections. The improvement of gradient flow is displayed with the existence of rampant skip connections of the pathways. The previous convolution layer's outcome is the similar dense section integrated by the matching upsampled outcome of the below dense section in the fusion layer that follows before every convolution layer. This is formulated in Eq. (17). Here the convolution process is given and the activation function is denoted as $V(\bullet)$. The variable $z^{j,k}$ is the feature map.

$$z^{j,k} = \begin{cases} I\left(z^{j-1,k}\right), k = 0 \\ I\left(\left[z^{j-1,k}\right], V\left(v^{j+1,k-1}\right)\right), k > 0 \end{cases} \tag{17}$$

Thus, the transformer and Unet++ networks are integrated to produce more accurate outcomes. The recommended transUnet++ network can discover the abnormalities even if the image is damaged or the region is too small to notice. The diagrammatic representation of transUnet++ is offered in Fig.4.

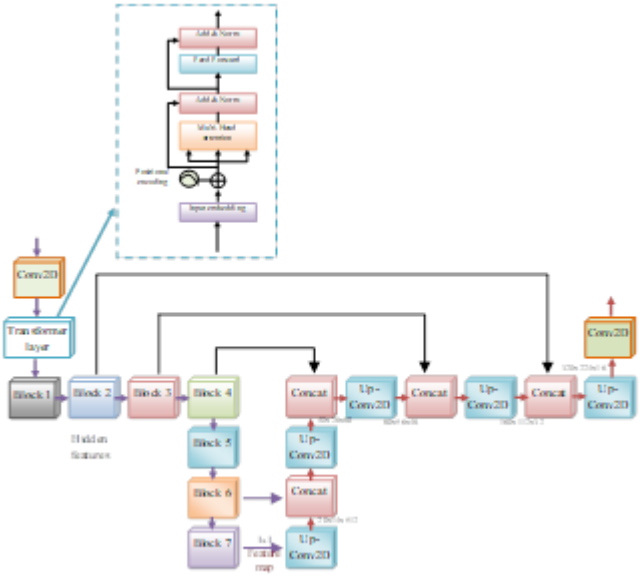

Figure 4 Diagrammatic representation of transUnet++ technique

B. MobileNetv3

MobileNetv3 [29] is adopted for the medical image segmentation process. The MobileNet is developed to minimize parameter utilization and make it effective for mobile systems. The MobileNet contains the new activation function, Inverted Residual Block (IRB), Squeeze and Excitation (SE) sections, and depth-wise convolutions. MobileNet produces highly accurate outcomes when contrasted to the other CNN frameworks. Most

importantly, the MobileNetv3 has the highest accuracy when contrasted to MobileNet variations. The MobileNet is integrated with some blocks named b-neck blocks. The MobileNetv1 exchanged normal convolutional tasks by the operations of depth-wise convolution in the entire block to minimize the parameter utilization. The IRB is employed to more minimization in the model's computational cost. To minimize the computations, the experts employed linear activations after performing the filtering task in input. Lastly, in MobileNetv3, the experts integrated the SE section. Nonetheless, unlike other techniques that integrate the SE sector as a private module of CNN, Inception, or ResNet, the MobileNetv3 joins it in parallel to the IRB connection. The integration of the SE sector enhanced the network size lightly yet improved the correctness and minimized the delay of the system. Within the SE section, the activation function is integrated which is formulated in Eq. (18).

$$af(y) = y\,\sigma(\alpha y) = \frac{y}{1+e^{-\alpha y}} \tag{18}$$

In this, the sigmoid function is pointed as $\sigma(\alpha y)$, and the trainable attribute is given as α. However, the computation of this function is very costly; hence the activation function is introduced which is given in Eq. (19).

$$i - af(y) = y\,\frac{\mathrm{Re}LU6(y+3)}{6} \tag{19}$$

Here, the variable $\mathrm{Re}LU6(y)$ is the ReLU's variation, whereby the activation function is restricted to the highest size of six. The functional block of MobileNetv3 is presented in Fig.5.

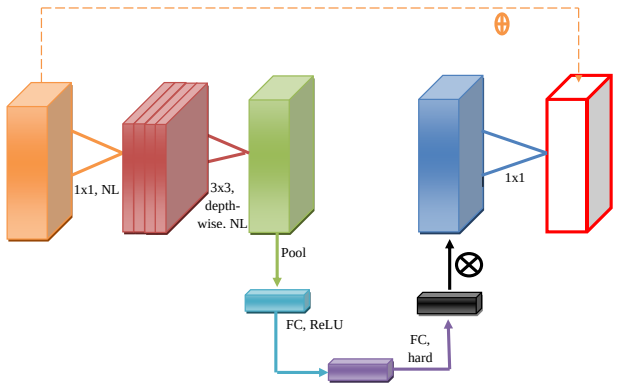

Figure 5 The functional block of MobileNetv3 for abnormality segmentation

C. Proposed TUnet++-MNetv3 for Segementation

A newly developed TUnet++-MNetv3 is recommended in this work for image segmentation. This network is composed of transUnet++ and MobileNetv3. The transUnet++ technique improves the accuracy rates and also focuses on the significant regions even if it is too small. When considering MobileNetv3, the computational burden of the network is relatively mitigated and the parameter utilization is also reduced. By observing the merits of these two techniques, the suggested work utilized these techniques and integrated them to improve the performance rates. Hence, the TUnet++-MNetv3 is constructed for segmenting the abnormalities present in the images. At first, the gathered necessary images are taken to the suggested network, where the encoder section of the Unet++ is replaced by the MobileNetV3 and Transformer layer. Further, the abnormalities that exist in the images are segmented by recommended technique. The suggested TUnet++-MNetv3-based abnormality segmentation improves the accuracy of the MS classification and also the computation time is highly reduced. Finally, the resultant segmented images are acquired and represented as S_c^{seg} for further process. The TUnet++-MNetv3-based abnormality segmentation is diagrammatically shown in Fig.6.

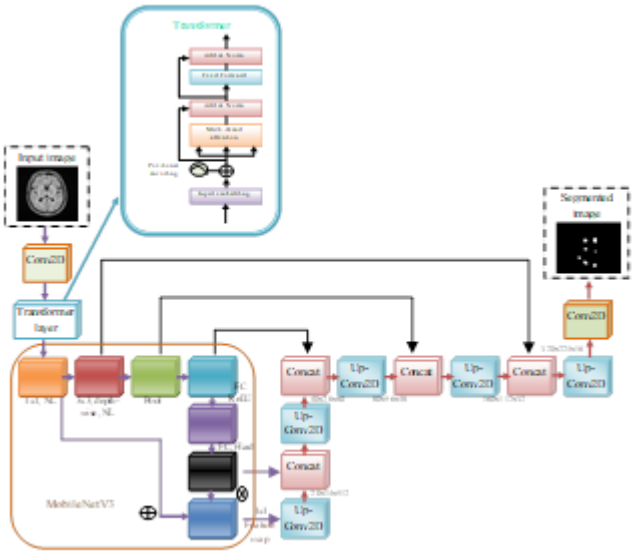

Figure 6 A diagrammatical representation of TUnet++-MNetv3-based abnormality segmentation

V. HYBRID DILATED CONVOLUTION-AIDED ADAPTIVE MOBILENET WITH PARAMETER TUNING FOR CLASSIFYING MULTIPLE SCLEROSIS

A. Hybrid Dilated Convolution

The hybrid dilated convolution [30] is supported in the MS classification. While taking the classification technique, the characteristics of spatial and spectral must be taken. To get the hyperspectral attributes, an advanced convolution provides better attention to continuous tasks that highly minimize the computational burden and the local convolution prevents the nearby region's spatial similarity. The dilated convolution is capable to enlarge the convolution domain's perception sector and grasp the data of multi-scale context. However, the conventional dilated convolution may cause two primary issues, such as the gridding effect that defines the interrupted kernels and long-ranged data that may be not related, this means that the approach was not sufficient in small instances. Hence, a hybrid dilated convolution is suggested. It includes numerous sizes of dilation rates that can efficiently rectify the mentioned issues. This hybrid dilated convolution includes three special features. First, the dilation rate's shape is resized in a zigzag format. Second, the stacked hybrid dilation convolution's dilation rates cannot have a general factor of more than one. Third, the hybrid dilated convolution fulfills the expression in Eq. (20).

$$N_j = \max\left[N_{j+1} - 2s_j, N_{j+1} - 2\left(N_{j+1} - s_j\right), s_j\right] \qquad (20)$$

Here, the dilation rate of j^{th} a layer is taken by, and the j^{th} layer's biggest dilation rate is denoted as N_j.

B. MobileNet

The MobileNet [31] is a lightweight Deep Neural Network with low latency and low power techniques that encounter the requirements of resource-constrained cases. The MobileNet is discovered on the streamlined framework, employing depth-wise and point-wise convolutions. The fundamental variation between the MobileNet and the streamlined framework is the convolution task, where the MobileNet contains the filtering process, and integrates the outcomes and inputs as two stages rather than a single stage. However, this architecture is highly rapid because of the minimized amount of attributes, whereby the 3x3 separable convolutions minimized the estimations by 9 times though a little minimization in accuracy. With the support of inception and depth-wise separable convolutions, the MobileNet minimizes the computation in the starting layers. To minimize the network

size and computation in MobileNet, the embedded point-wise convolution is supported. Hence, the MobileNet minimizes the cognitive and execution complexities effectively to classify diseases from medical images.

C. Recommended HDC-AMNet for Classification

The HDC-AMNet is developed in this framework for diagnosing the MS. This network is the integration of hybrid dilated convolution and MobileNet. The hybrid dilated convolution includes various dilation rates. With these dilation rates, the classification process is performed effectively. In addition to that, the MobileNet increases the accuracy and minimizes the parameter utilization of the model. However, the parameters present in the MobileNet may consume more time to perform the process and also, the network attributes may create overfitting issues while executing huge amounts of images. Thus, optimizing these parameters in MobileNet is a very significant concept. This parameter utilization task makes the presented work a unique and promising one. For optimizing the MobileNet parameters the recommended ESCO is employed. This ESCO has attained better abilities by updating its random factor than the traditional SCO. Moreover, it increases the convergence rates hence it is easier to discover the optimal solutions. Thus, an effective HDC-AMNet is implemented for classifying the MS. In this process, initially, the segmented images S_c^{seg} attained from the TUnet++-MNetv3 technique are fed into the HDC-AMNet technique, where the MS is categorized with the support of hybrid dilated convolution and MobileNet. The objective function of this parameter tuning operation is given by Eq. (21).

$$ob = \underset{\left\{hn^{MNet}, ep^{MNet}, af^{MNet}\right\}}{\arg\min} \left[\frac{1}{A} + \frac{1}{P} + FNR + FDR + FPR\right] \qquad (21)$$

Here, MobileNet's activation function and hidden neuron count are noted hn^{MNet} *and* af^{MNet}. The MobileNet's number of epochs is indicated as ep^{MNet}. The MobileNet's activation function and hidden neuron count range from [5-255], and [0-4] respectively. The MobileNet's number of epochs is varied from [5-50]. The 'False Positive Rate (FPR), False Negative Rate (FNR), and False Discovery Rate (FDR)' are minimized with the help of recommended ESCO. Besides, the Precision (P), and Accuracy (A) are maximized by the same ESCO.

Accuracy: It defines how the same achieved outcomes are to the desired outcomes. It is given in Eq. (22).

$$A = \frac{fe + hg}{fe + hg + ba + dc} \qquad (22)$$

Precision: It is explained as the localized solutions and the related factors of anomaly recognized. This is estimated by Eq. (23).

$$P = \frac{fe}{fe + hg} \qquad (23)$$

FNR: It is the probability that a true positive will be skipped in the experiment. This is measured by Eq. (24).

$$FNR = \frac{ba}{ba + dc} \qquad (24)$$

FDR: It is the factor describing the value of both TP and FP and FP. It is shown in Eq. (25).

$$FDR = \frac{ba}{fe + ba} \qquad (25)$$

FPR: It is the variable that is selected by mistake. This is illustrated by Eq. (26).

$$FPR = \frac{ba}{ba + fe} \tag{26}$$

Here, the "true and negative positive" factors are noted fe *and* hg. The "false negative and false positive" factors are noted as dc *and* ba.

Thus, the MS classified outcome is obtained by the developed HDC-AMNet and it is depicted in Fig.7.

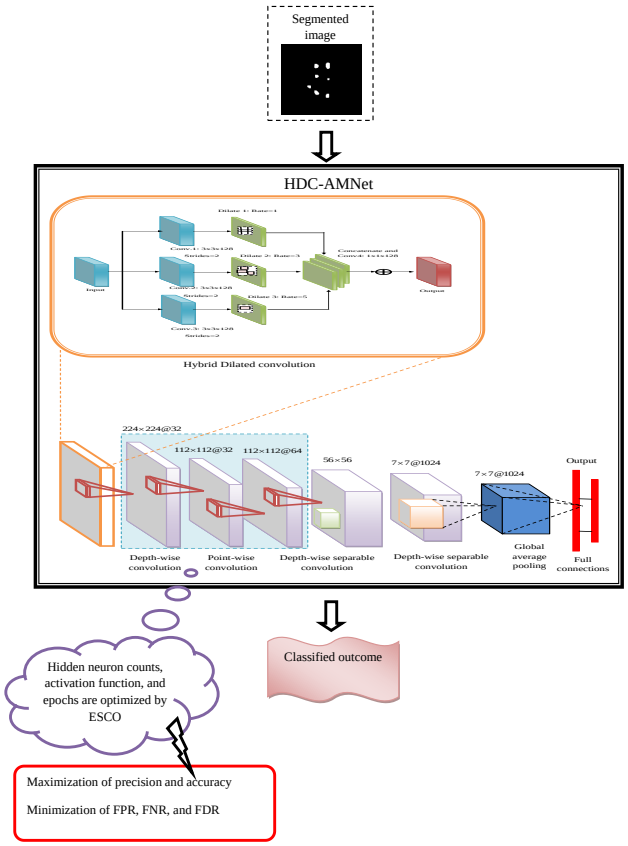

Figure 6 Depiction of HDC-AMNet-based MS classification framework

VI. Results and Discussions

A. Experimental setup

The designed MS classification technique has been executed in Python. With this paradigm, promising solutions were achieved for the developed MS classification process. The ESCO process's chromosome length was 3 and the population count was 10. The utmost iteration of the ESCO was 50. The classical algorithms such as "Dingo Optimization Algorithm (DOA) [32], Reptile Search Optimizer (RSA) [33], Tomtit Flock Metaheuristic Optimization Algorithm (TFMOA) [34], and SCO [26]" are taken for performance evaluation. The existing segmentation approaches like "Unet [35], Unet3+ [36], TransUnet [37], and TransUnet with MobileNetv3 [37] [29]" were employed for the analysis. The conventional classifiers including "CNN [38], Densenet [39], Residual Attention Network (RAN) [40], and HDC with MobileNet [30] [31]" are taken for experiment validation.

B. Resultant images

The developed MS classification process has been executed and the TUnet++-MNetv3-based segmented images were displayed in Fig.8 over conventional techniques.

Description	1	2	3	4	5
"FLAIR"					
"Image"	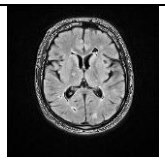	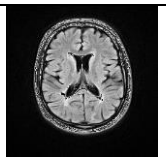	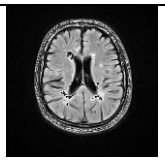	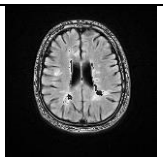	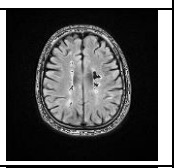
"Ground truth"	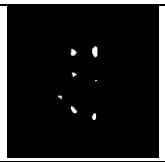	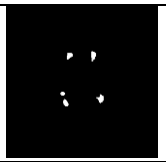			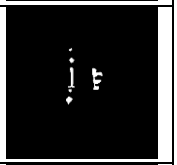
"Segmented"	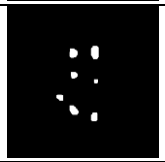	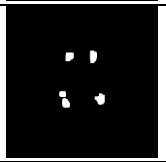	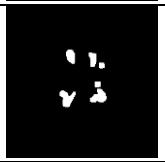	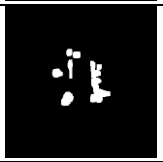	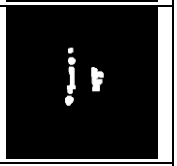
"T1"					
"Image"	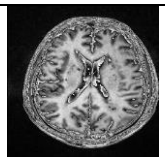		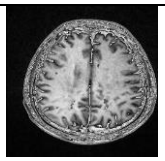	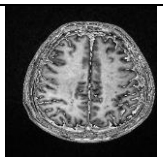	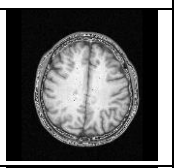
"Ground truth"		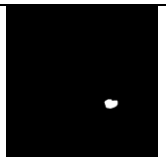		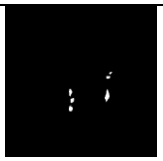	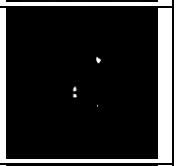
"Segmented"				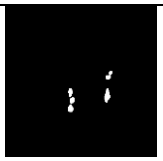	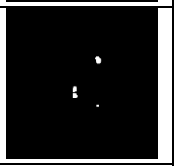
"T2"					
"Image"	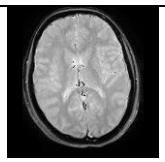	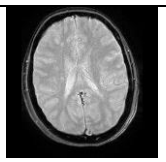	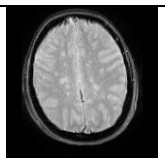	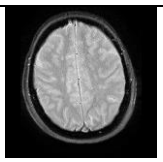	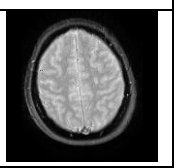
"Ground truth"		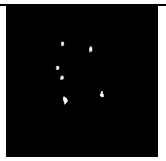			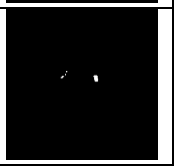
"Segmented"			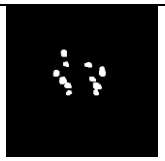		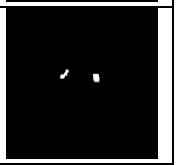

Figure 7 Resultant images of the TUnet++-MNetv3-based segmentation process

C. Performance metrics

The necessary performance factors employed in the presented task are measured as follows.

Accuracy is measured by Eq. (22).

Precision is determined by Eq. (23).

FNR is calculated by Eq. (24).

FDR is estimated by Eq. (25).

FPR is given by Eq. (26).

MCC is given in Eq. (27).

$$MCC = \frac{dc \times hg - dc \times fe}{\sqrt{(dc + fe)(dc + hg)(fe + ba)(fe + dc)}} \quad (27)$$

Recall is given by Eq. (28).

$$\mathrm{Re} = \frac{hg}{hg + dc} \quad (28)$$

Specificity is estimated by Eq. (29).

$$spec = \frac{ba}{ba + dc} \quad (29)$$

Sensitivity is derived by Eq. (30).

$$Sen = \frac{fe}{fe + hg} \quad (30)$$

F1 score is expressed in Eq. (31).

$$F1 - Score = 2 \times \frac{hg \times ba}{hg + ba} \quad (31)$$

NPV is given by Eq. (32).

$$NPV = \frac{fe}{fe + dc} \quad (32)$$

The dice coefficient is formulated by Eq. (33).

$$Dce(m, y) = \frac{2(m \cap y)}{(m + y)} \quad (33)$$

Jaccard is derived in Eq. (34).

$$jcd(m, y) = \frac{(m \cap y)}{(m \cup y)} \quad (34)$$

Here, the factors m *and* y specify the two data sources. Further, the intersection and union operations are given as $\cap$ *and* $\cup$.

D. Confusion matrix analysis of recommended MS classification

Fig.9 displays the confusion matrix estimation of the presented MS classification approach using various images including FLAIR, T1, and T2. The confusion matrix supports to determination the accuracy of the model by employing actual and predicted values. Fig.9 (b) shows that, when analyzing the recommended MS classification using T1 images, the accuracy is maximized by 95.87%. Hence, it is confirmed that the developed MS classification model achieved high-accuracy outcomes.

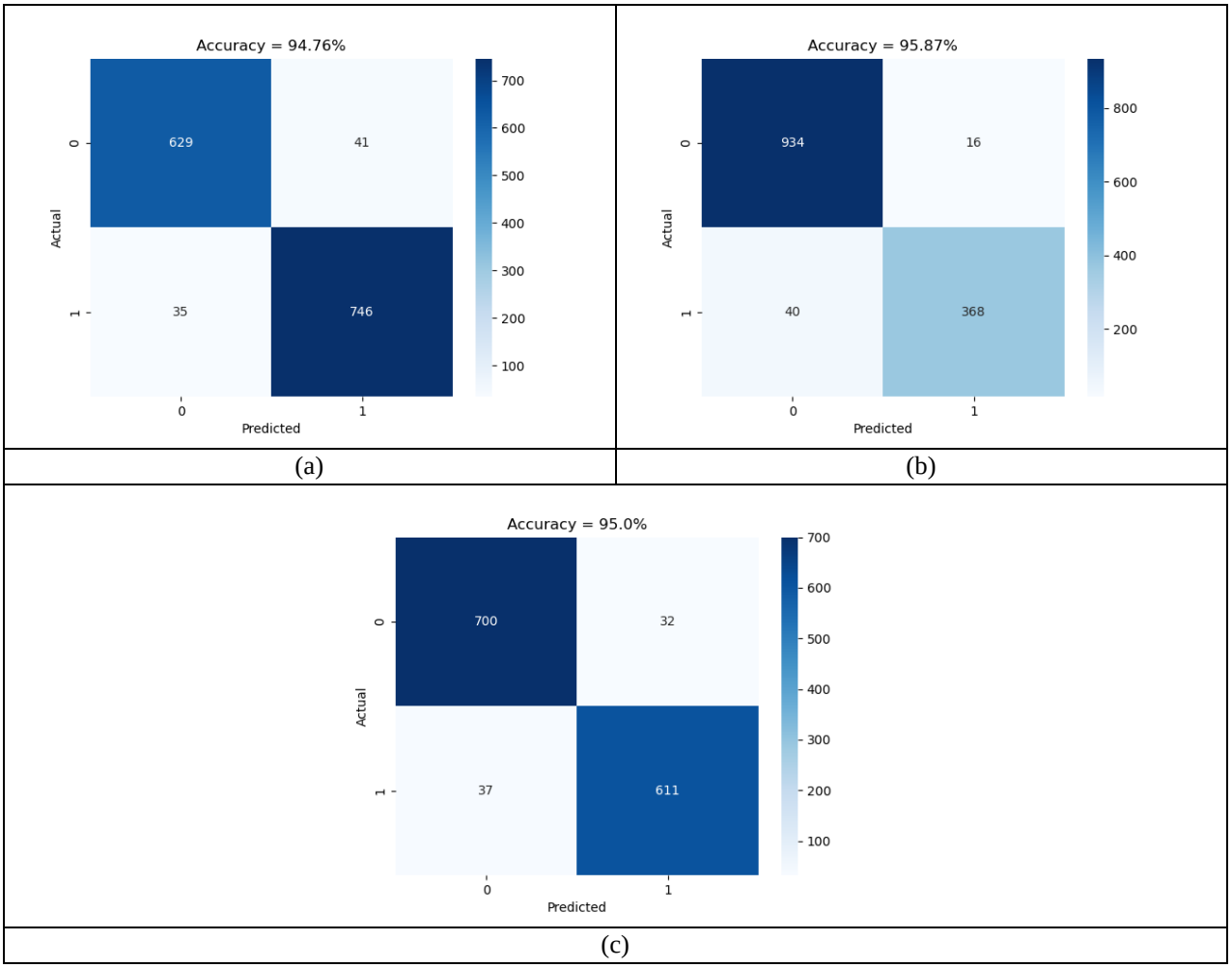

Figure 8 Confusion matrix analysis of recommended MS classification technique concerning " (a) FLAIR images, (b) T1 images, and (c) T3 images"

E. Convergence analysis of recommended ESCO

The developed ESCO model's convergence is evaluated over distinct traditional optimization techniques and given in Fig.10. The ESCO's convergence is analyzed with various images including FLAIR, T1, and T2. The designed ESCO model's convergence is enhanced by 45.83% of DOA-HDC-AMNet, 20.83% of RSA-HDC-AMNet, 33.33% of TFMO-HDC-AMNet, and 25% of SCO-HDC-AMNet accordingly in Fig.10 (a) for 30th iteration. Hence, it is described that the developed ESCO has attained a very low-cost function that improves the convergence rates of the suggested task. With the support of these improved convergence rates, the implemented work can easily explore the optimal outcomes.

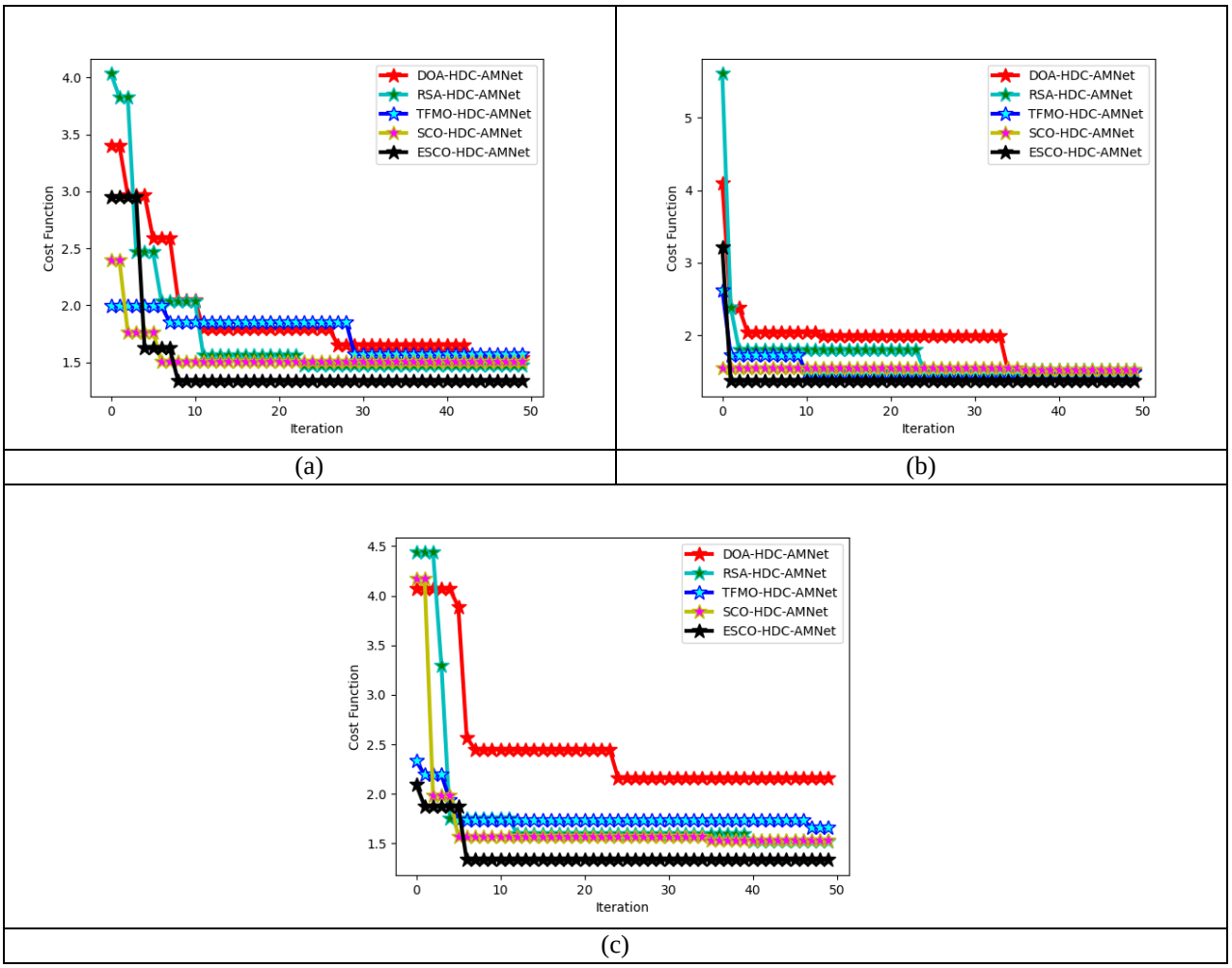

Figure 9 Confusion matrix analysis of recommended ESCO approach over classical algorithms concerning " (a) FLAIR images, (b) T1 images, and (c) T3 images"

F. Statistical analysis of recommended ESCO

Table II depicts the statistical illustration of the suggested ESCO technique over traditional optimization approaches for three kinds of images including FLAIR, T1, and T2. The performance rate of the designed ESCO is improved by 77.85% of DOA-HDC-AMNet, 28.57% of RSA-HDC-AMNet, 26.42% of TFMO-HDC-AMNet, and 20% of SCO-HDC-AMNet appropriately when analyzing the mean factor for T2 images. When analyzing other images such as FLAIR, and T1, the recommended ESCO provides improved statistical rates. Thus, this analysis highlighted that the recommended ESCO can attain very promising outcomes and with this analysis, it is proved that the implemented work effectively optimizes the parameters by utilizing the ESCO approach.

TABLE II. **STATISTICAL ANALYSIS OF RECOMMENDED ESCO MODEL OVER TRADITIONAL ALGORITHMS USING FLAIR, T1, AND T2 IMAGES**

TERMS	DOA-HDC-AMNet [32]	RSA-HDC-AMNet [33]	TFMO-HDC-AMNet [34]	SCO-HDC-AMNet [26]	ESCO-HDC-AMNet
"FLAIR"					
"Worst"	3.402957522	4.0325501	1.993227885	2.396831333	2.951130917
"Best"	1.539930929	1.474005389	1.568778196	1.507672777	1.332324131
"Mean"	1.910145456	1.755604162	1.752634823	1.563742194	1.484932971
"Median"	1.791857645	1.474005389	1.851581993	1.507672777	1.332324131
"Std"	0.47973277	0.6051505	0.163122992	0.183671008	0.439347222
"T1"					

"Worst"	4.090945326	5.604627631	2.623415255	1.545763261	3.215662696
"Best"	1.494782685	1.521605464	1.486292076	1.516693354	1.365310767
"Mean"	1.895958279	1.74037267	1.552467618	1.537623687	1.402317806
"Median"	1.986006761	1.521605464	1.486292076	1.545763261	1.365310767
"Std"	0.405373461	0.577057905	0.17877908	0.013052356	0.25904927
"T2"					
"Worst"	4.066976758	4.435854826	2.331005027	4.171251737	2.094335824
"Best"	2.158493889	1.519032775	1.665371344	1.533375575	1.334048574
"Mean"	2.490681228	1.809559351	1.771160336	1.685928024	1.403446286
"Median"	2.158493889	1.596453598	1.731303004	1.566720768	1.334048574
"Std"	0.587882802	0.707551008	0.139718323	0.517598098	0.190032587

G. ROC analysis of recommended MS classification

The developed MS classification model's ROC is validated over conventional classifiers for three kinds of images such as FLAIR, T1, and T2. This estimation is displayed in Fig.11. When analyzing the T1 image in Fig. 11 (b), the developed MS classification is enriched by 6.25% of CNN, 3.12% of DenseNet, 5.2% of RAN, and 2.08% of ADC-AMNet correspondingly for 0.2nd FPR value. The suggested technique provides improved performance rates for other images also. With this estimation, it is proved that the designed MS classification framework attained more effectiveness than the conventional classification models. Moreover, the error rates of the developed technique are also minimized and this is proved by this estimation.

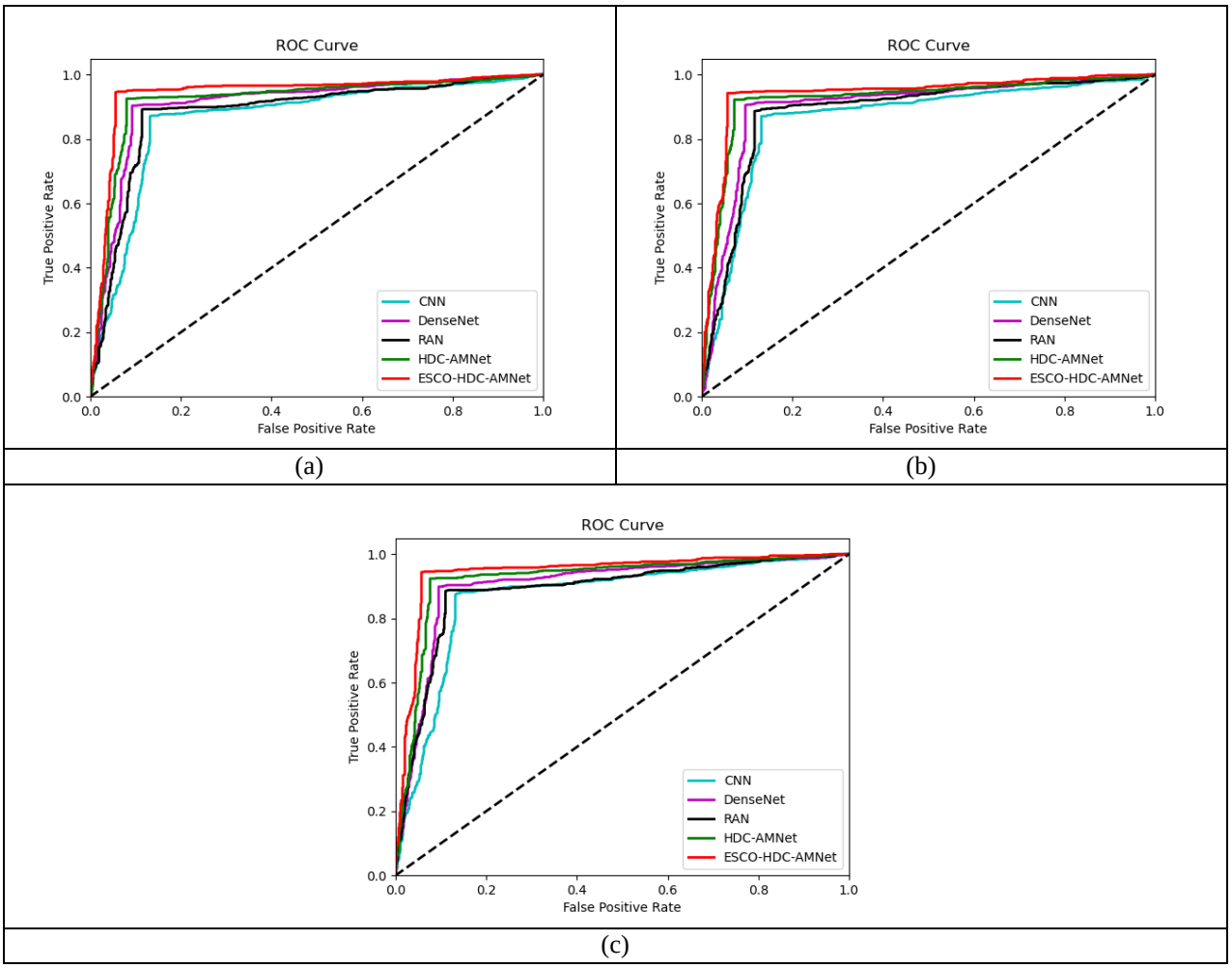

Figure 10 ROC analysis of suggested MS classification model over existing classifiers concerning " (a) FLAIR images, (b) T1 images, and (c) T3 images"

H. Performance evaluation of the suggested segmentation task

The recommended segmentation approach is performance is validated using FLAIR, T1, and T2 images. This validation is given from Fig.12 to Fig.14. When utilizing median factor FLAIR images, the recommended segmentation task's accuracy is maximized by 5.26% of UNet, 2.10% of UNet3+, 3.15% of TransUnet, and 1.05% of TUnet++-MNetv3 correspondingly in Fig.12 (a). Hence, it is guaranteed that the implemented segmentation task achieved higher accuracy in segmenting the abnormalities that exist in the images. In addition to that, the developed segmentation process attained higher Jaccard and dice coefficients than the other traditional techniques. This ensures that the developed segmentation process relatively enhances the efficacy of the recommended MS classification technique.

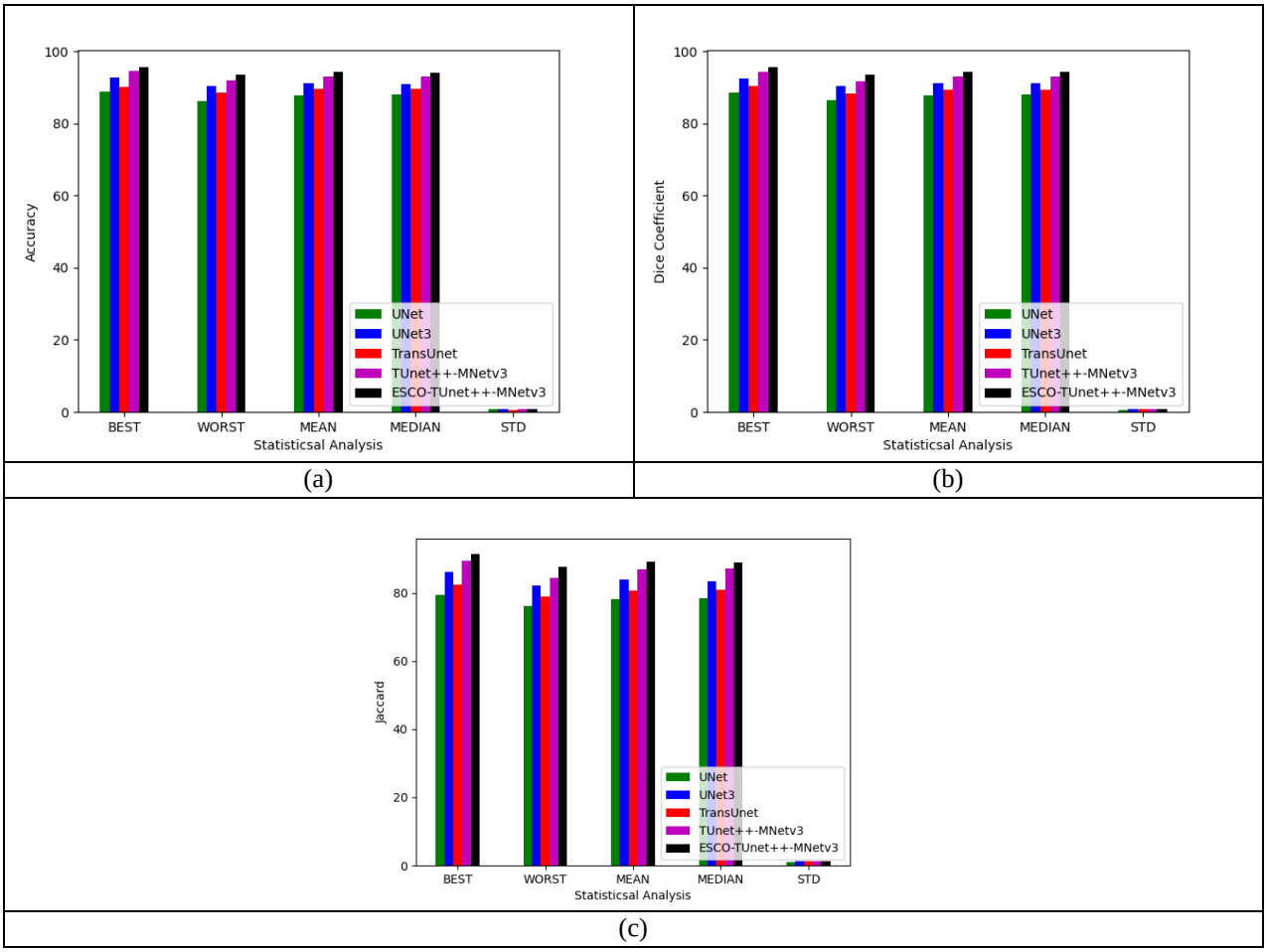

Figure 11 Performance evaluation of suggested segmentation process over existing techniques using FLAIR images concerning " (a) Accuracy, (b) Dice coefficient, and (c) Jaccard"

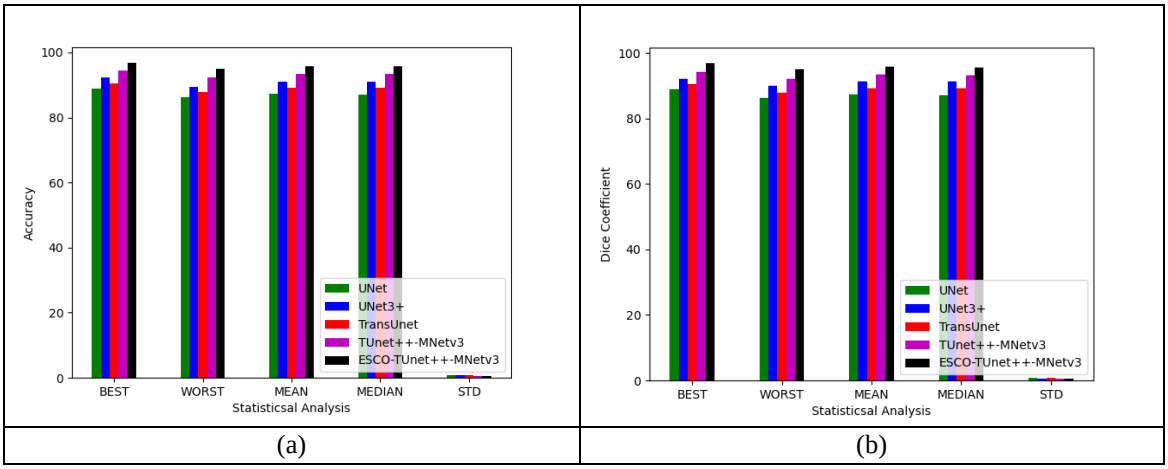

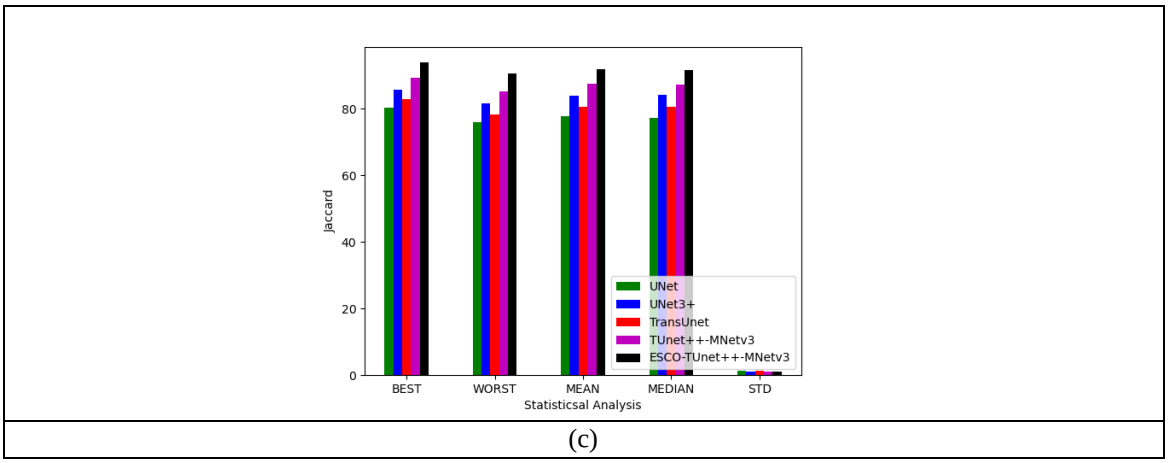

(c)

Figure 12 Performance evaluation of suggested segmentation process over existing techniques using T1 images concerning " (a) Accuracy, (b) Dice coefficient, and (c) Jaccard"

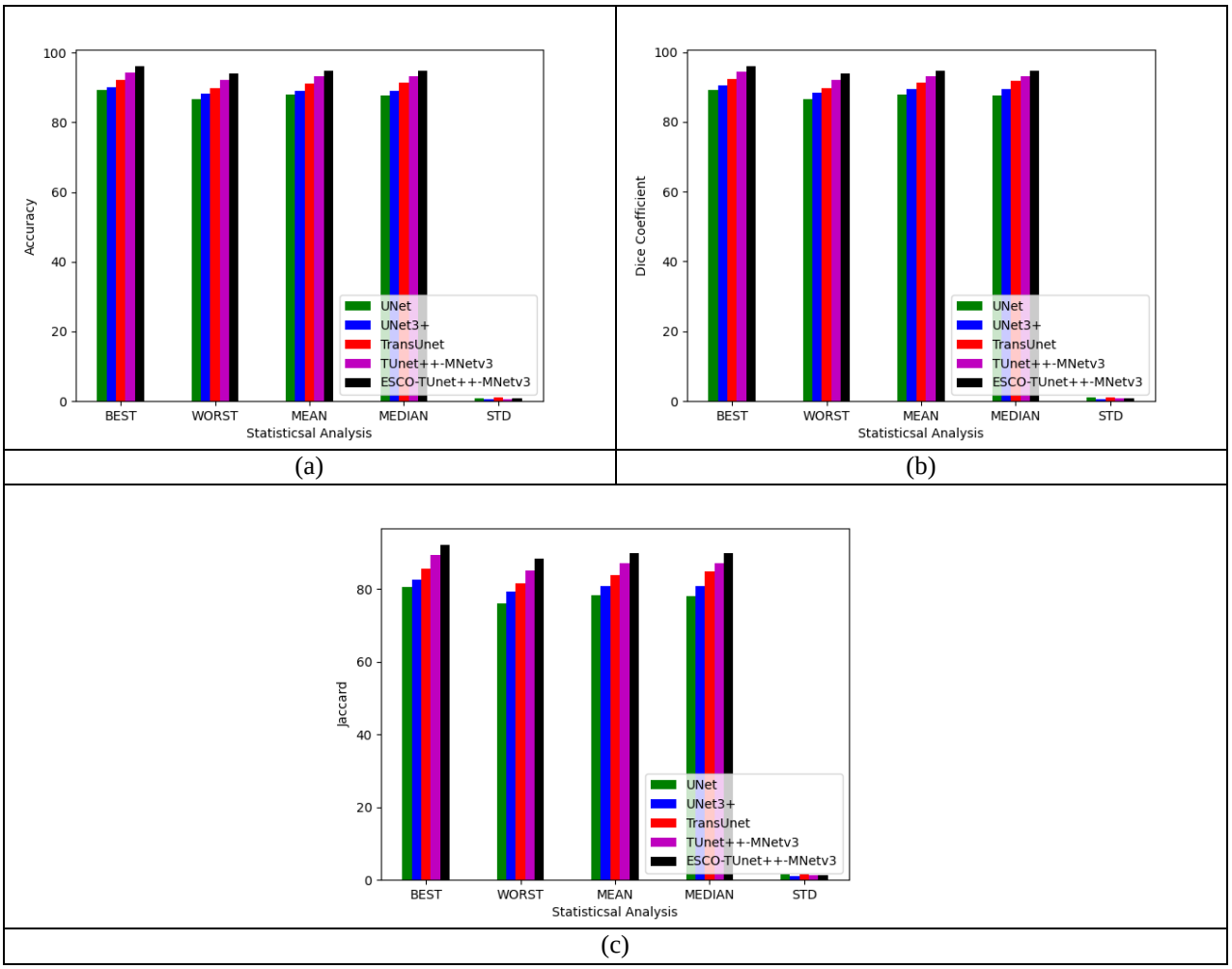

(a) (b)

(c)

Figure 13 Performance evaluation of suggested segmentation process over existing techniques using T2 images concerning " (a) Accuracy, (b) Dice coefficient, and (c) Jaccard"

I. Performance evaluation of recommended MS classification over diverse algorithms

From Fig.15 to Fig.17, the suggested MS classification task's performance is estimated over multiple existing algorithms using three images such as FLAIR, T1, and T2. Some of the evaluation factors are involved in this analysis. The recommended MS classification task's precision is enhanced by 6.80% of DOA-HDC-AMNet, 3.56% of RSA-HDC-AMNet, 4.92% of TFMO-HDC-AMNet, and 1.98% of SCO-HDC-AMNet respectively for

the 48th batch size in Fig.15 (g) for FLAIR images. The implemented classification technique offers an enhanced classification rate for other T1 and T2 images also than other algorithms. This evaluation guaranteed that the developed MS classification approach attained improved outcomes than the classical mechanisms.

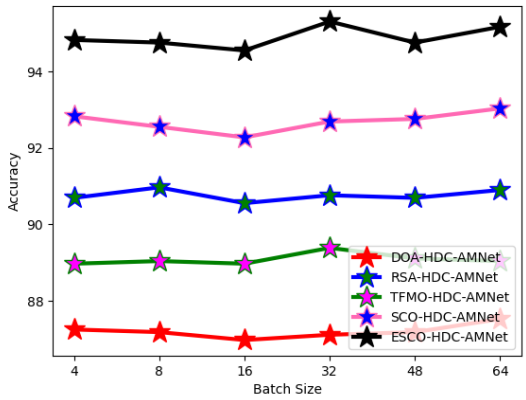

(a)

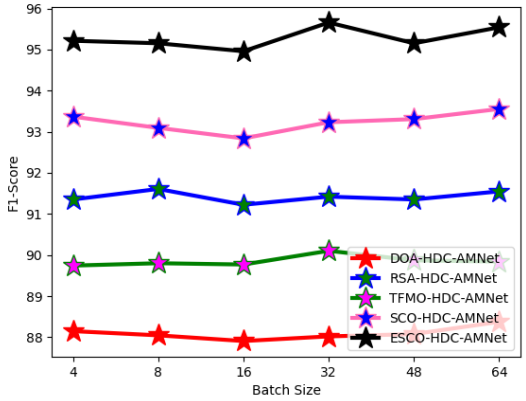

(b)

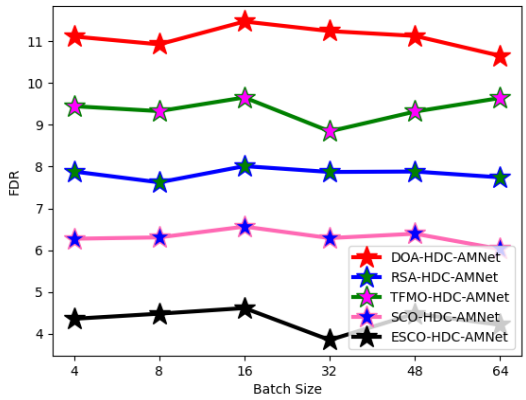

(c)

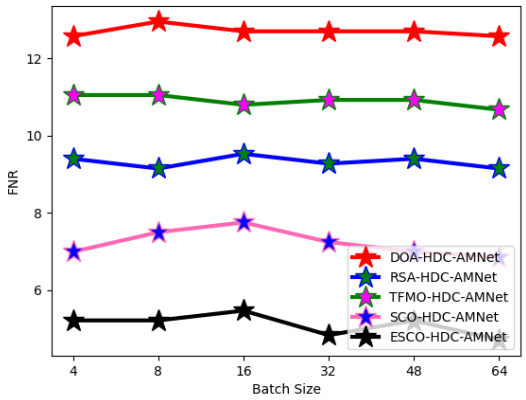

(d)

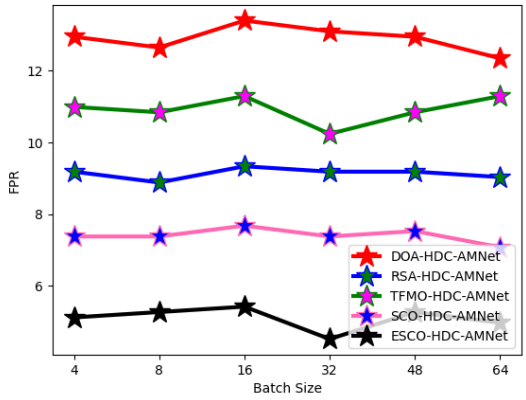

(e)

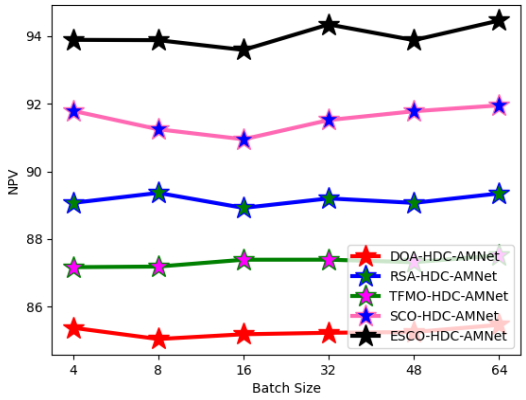

(f)

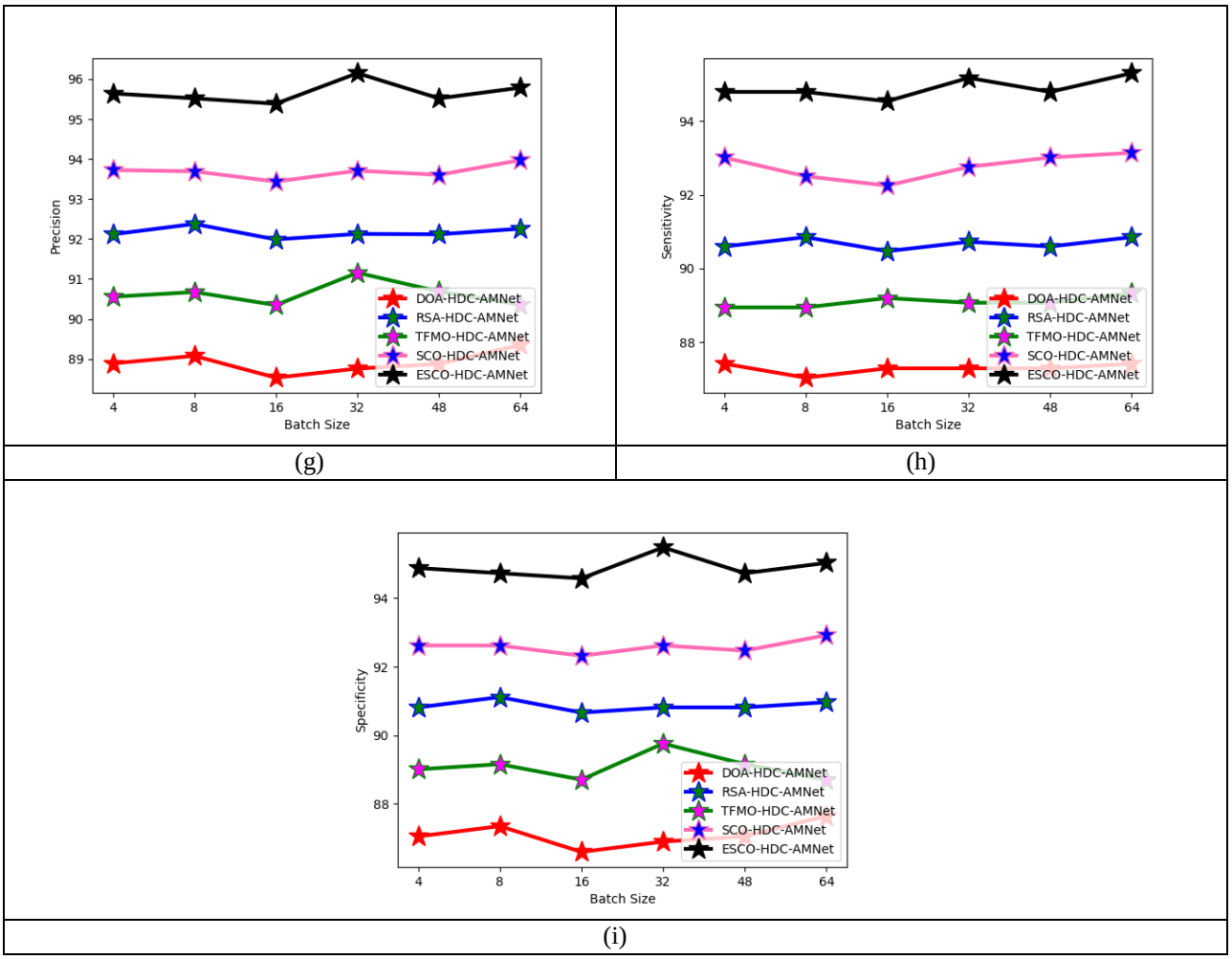

Figure 14 Performance evaluation of designed MS classification technique over existing algorithms using FLAIR images concerning "(a) Accuracy, (b) F1-score, (c) FDR, (d) FNR, (e) FPR, (f) NPV, (g) Precision, (h) Sensitivity, and (i) Selectivity"

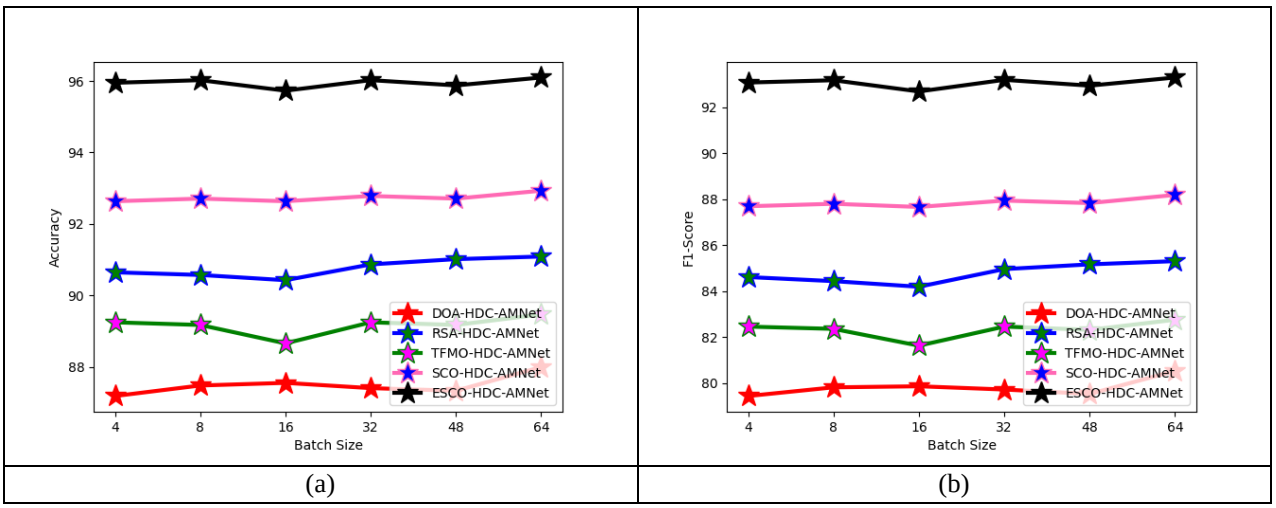

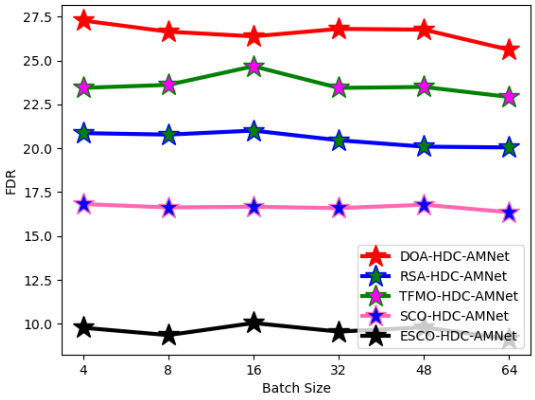
FDR
Batch Size
DOA-HDC-AMNet
RSA-HDC-AMNet
TFMO-HDC-AMNet
SCO-HDC-AMNet
ESCO-HDC-AMNet

(c)

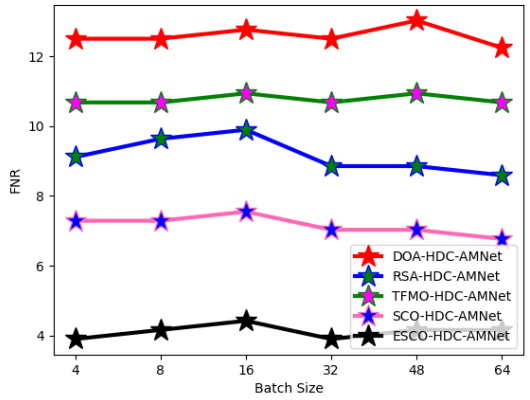
FNR
Batch Size
DOA-HDC-AMNet
RSA-HDC-AMNet
TFMO-HDC-AMNet
SCO-HDC-AMNet
ESCO-HDC-AMNet

(d)

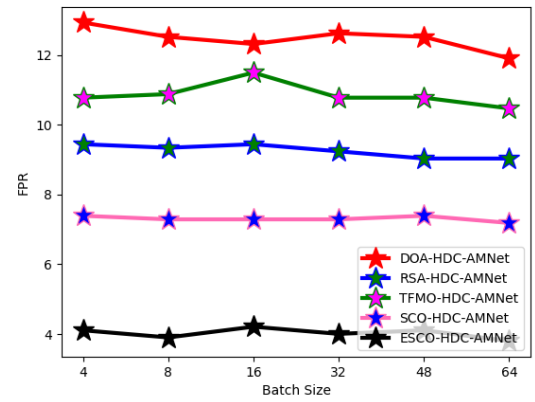
FPR
Batch Size
DOA-HDC-AMNet
RSA-HDC-AMNet
TFMO-HDC-AMNet
SCO-HDC-AMNet
ESCO-HDC-AMNet

(e)

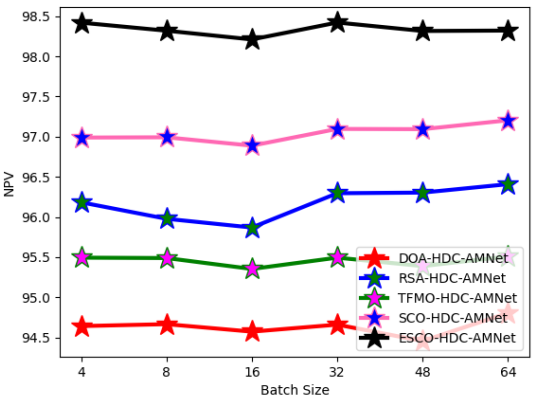
NPV
Batch Size
DOA-HDC-AMNet
RSA-HDC-AMNet
TFMO-HDC-AMNet
SCO-HDC-AMNet
ESCO-HDC-AMNet

(f)

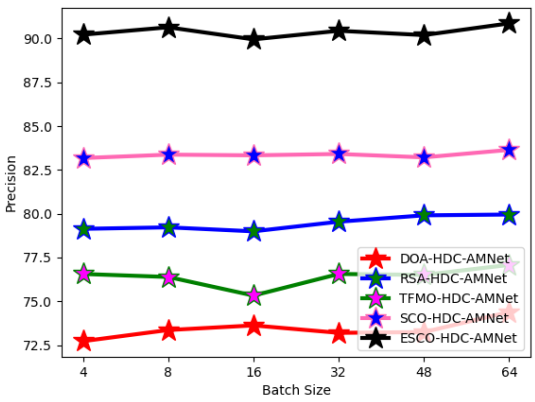
Precision
Batch Size
DOA-HDC-AMNet
RSA-HDC-AMNet
TFMO-HDC-AMNet
SCO-HDC-AMNet
ESCO-HDC-AMNet

(g)

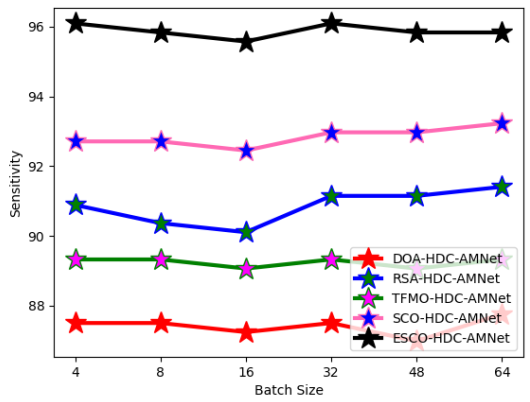
Sensitivity
Batch Size
DOA-HDC-AMNet
RSA-HDC-AMNet
TFMO-HDC-AMNet
SCO-HDC-AMNet
ESCO-HDC-AMNet

(h)

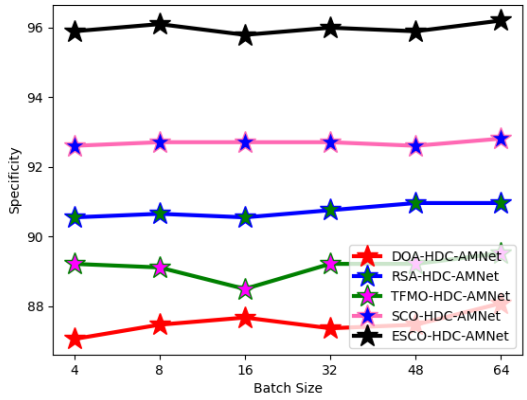

(i)

Figure 15 Performance evaluation of designed MS classification technique over existing algorithms using T1 images concerning "(a) Accuracy, (b) F1-score, (c) FDR, (d) FNR, (e) FPR, (f) NPV, (g) Precision, (h) Sensitivity, and (i) Selectivity"

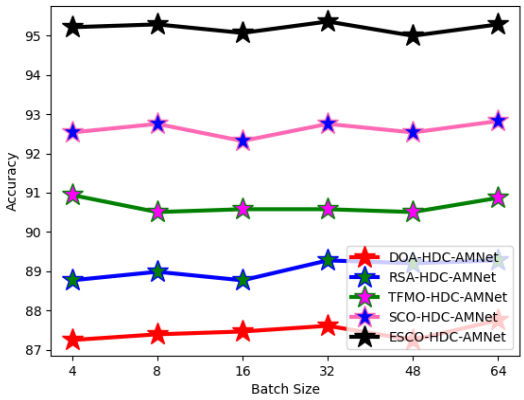

(a)

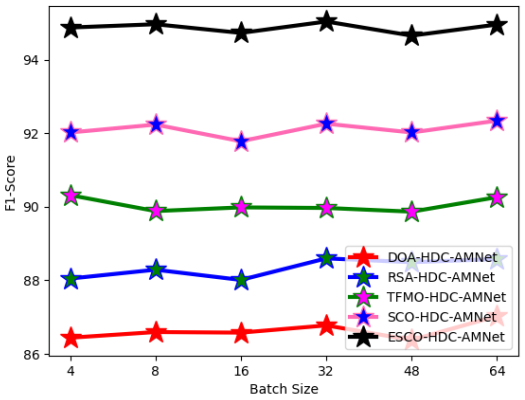

(b)

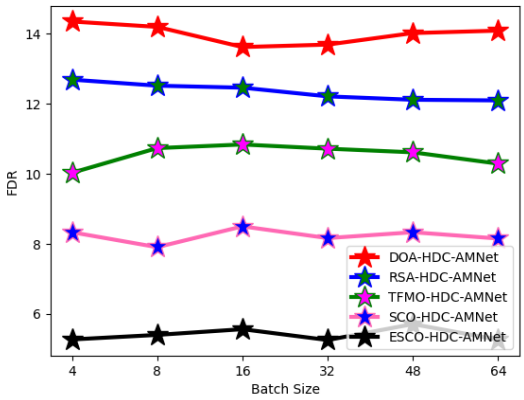

(c)

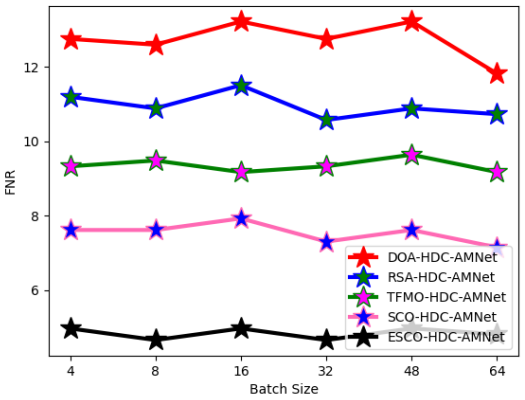

(d)

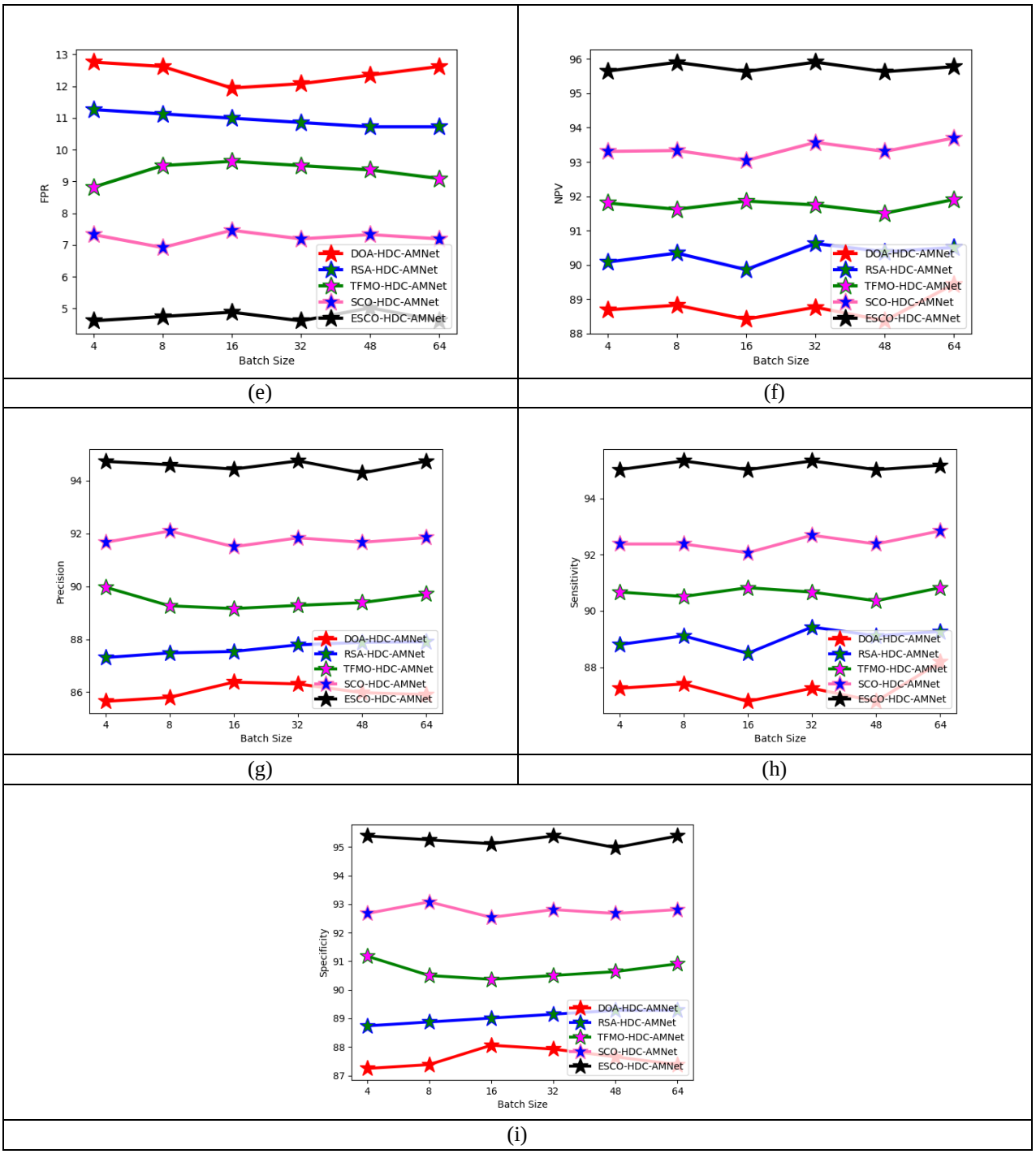

Figure 16 Performance evaluation of designed MS classification technique over existing algorithms using T2 images concerning "(a) Accuracy, (b) F1-score, (c) FDR, (d) FNR, (e) FPR, (f) NPV, (g) Precision, (h) Sensitivity, and (i) Selectivity"

J. Performance evaluation of recommended MS classification over diverse classifiers

The suggested MS classification approach's performance is experimented with over conventional classifiers using three kinds of images such as FLAIR, T1, and T2. This performance evaluation is shown from Fig.18 to Fig.20. From Fig.19 (e), the implemented MS classification technique's FPR is reduced by 21% of CNN, 13.6% of DenseNet, 16.3% of RAN, and 5.78% of ADC-AMNet appropriately for 32nd batch size when using T1 images. The designed framework obtained effective outcomes for FLAIR, and T2 images also over traditional techniques. Therefore, it is guaranteed that the recommended MS classification model attained very low error rates than the classical models.

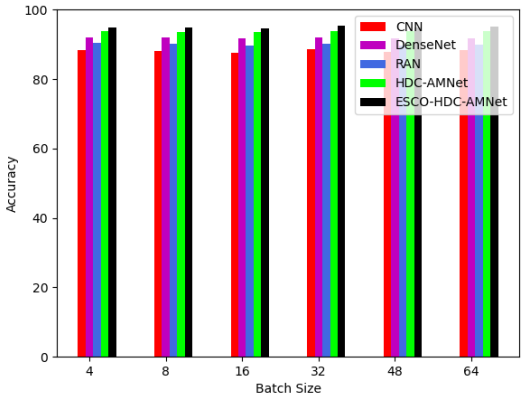
Accuracy
Batch Size
CNN
DenseNet
RAN
HDC-AMNet
ESCO-HDC-AMNet

(a)

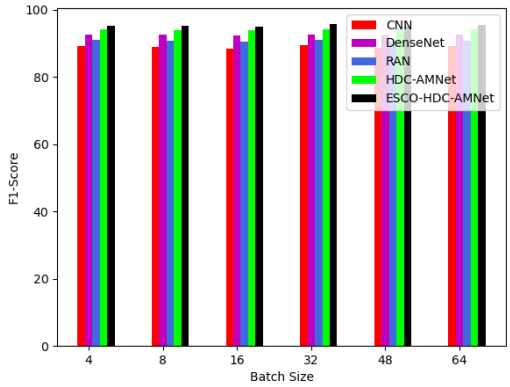
F1-Score
Batch Size
CNN
DenseNet
RAN
HDC-AMNet
ESCO-HDC-AMNet

(b)

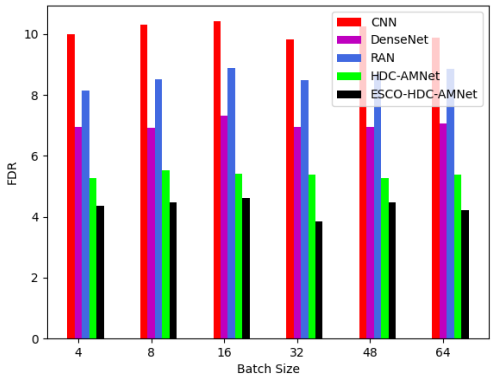
FDR
Batch Size
CNN
DenseNet
RAN
HDC-AMNet
ESCO-HDC-AMNet

(c)

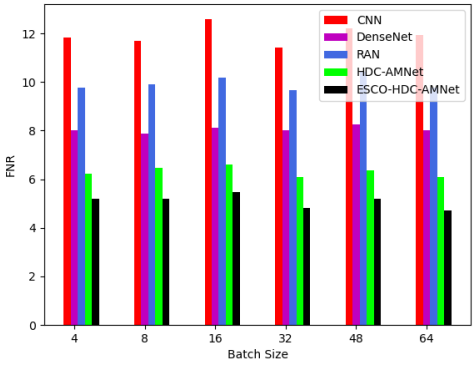
FNR
Batch Size
CNN
DenseNet
RAN
HDC-AMNet
ESCO-HDC-AMNet

(d)

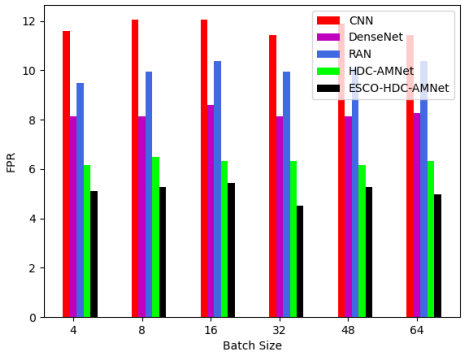
FPR
Batch Size
CNN
DenseNet
RAN
HDC-AMNet
ESCO-HDC-AMNet

(e)

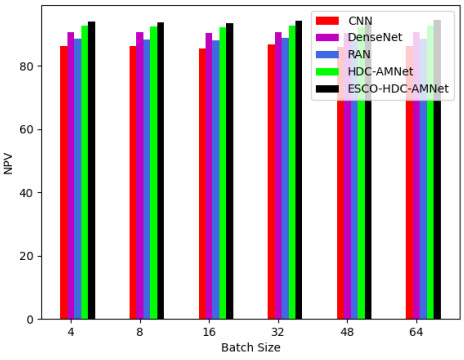
NPV
Batch Size
CNN
DenseNet
RAN
HDC-AMNet
ESCO-HDC-AMNet

(f)

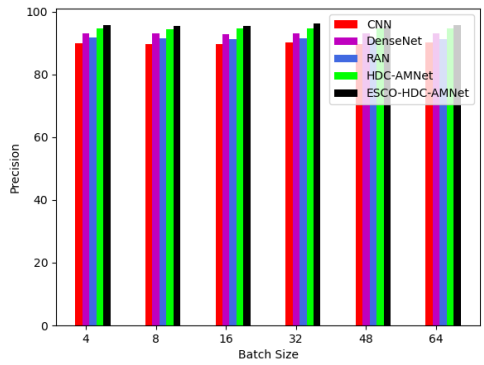
Precision
Batch Size
CNN
DenseNet
RAN
HDC-AMNet
ESCO-HDC-AMNet

(g)

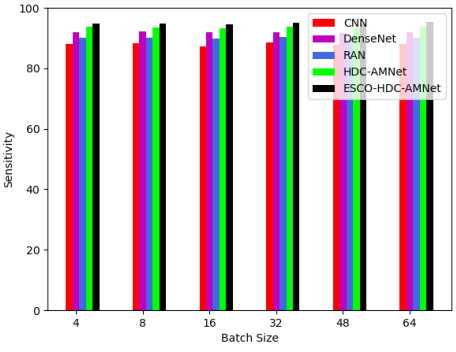
Sensitivity
Batch Size
CNN
DenseNet
RAN
HDC-AMNet
ESCO-HDC-AMNet

(h)

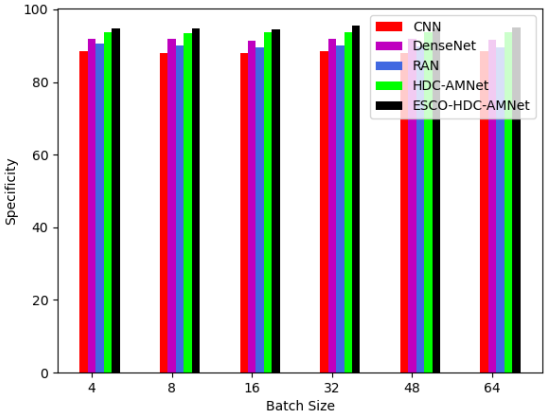

(i)

Figure 17 Performance evaluation of designed MS classification technique over existing techniques using FLAIR images concerning "(a) Accuracy, (b) F1-score, (c) FDR, (d) FNR, (e) FPR, (f) NPV, (g) Precision, (h) Sensitivity, and (i) Selectivity"

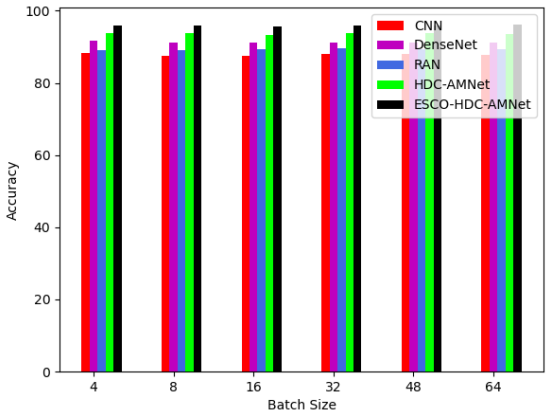

(a)

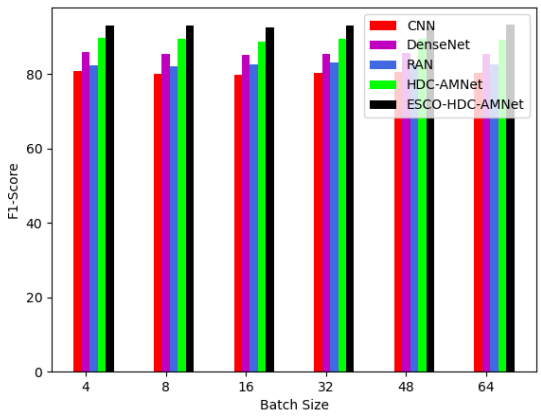

(b)

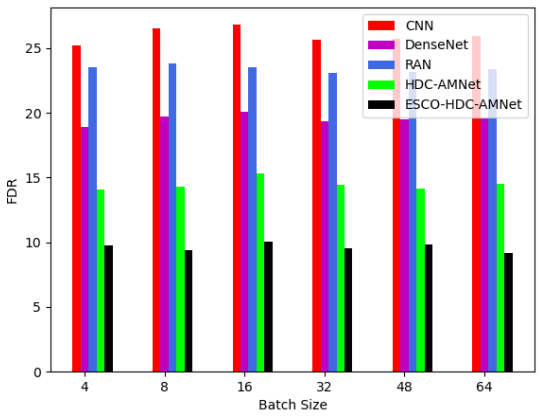

(c)

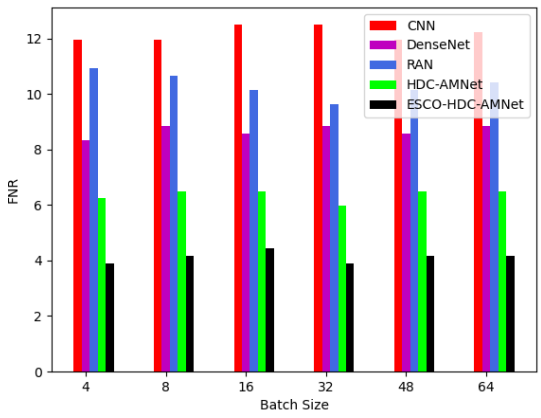

(d)

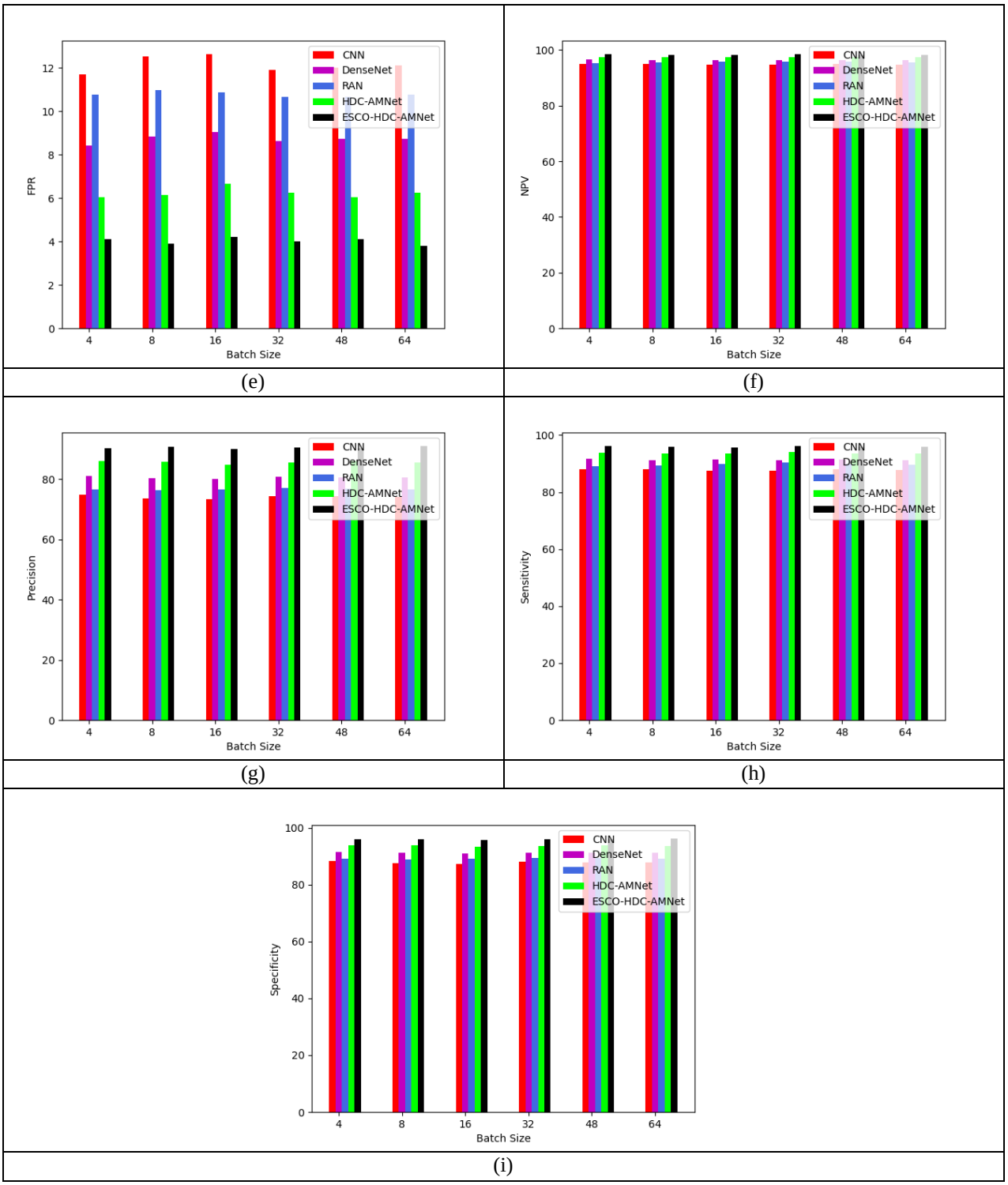

Figure 18 Performance evaluation of designed MS classification technique over existing techniques using T1 images concerning "(a) Accuracy, (b) F1-score, (c) FDR, (d) FNR, (e) FPR, (f) NPV, (g) Precision, (h) Sensitivity, and (i) Selectivity"

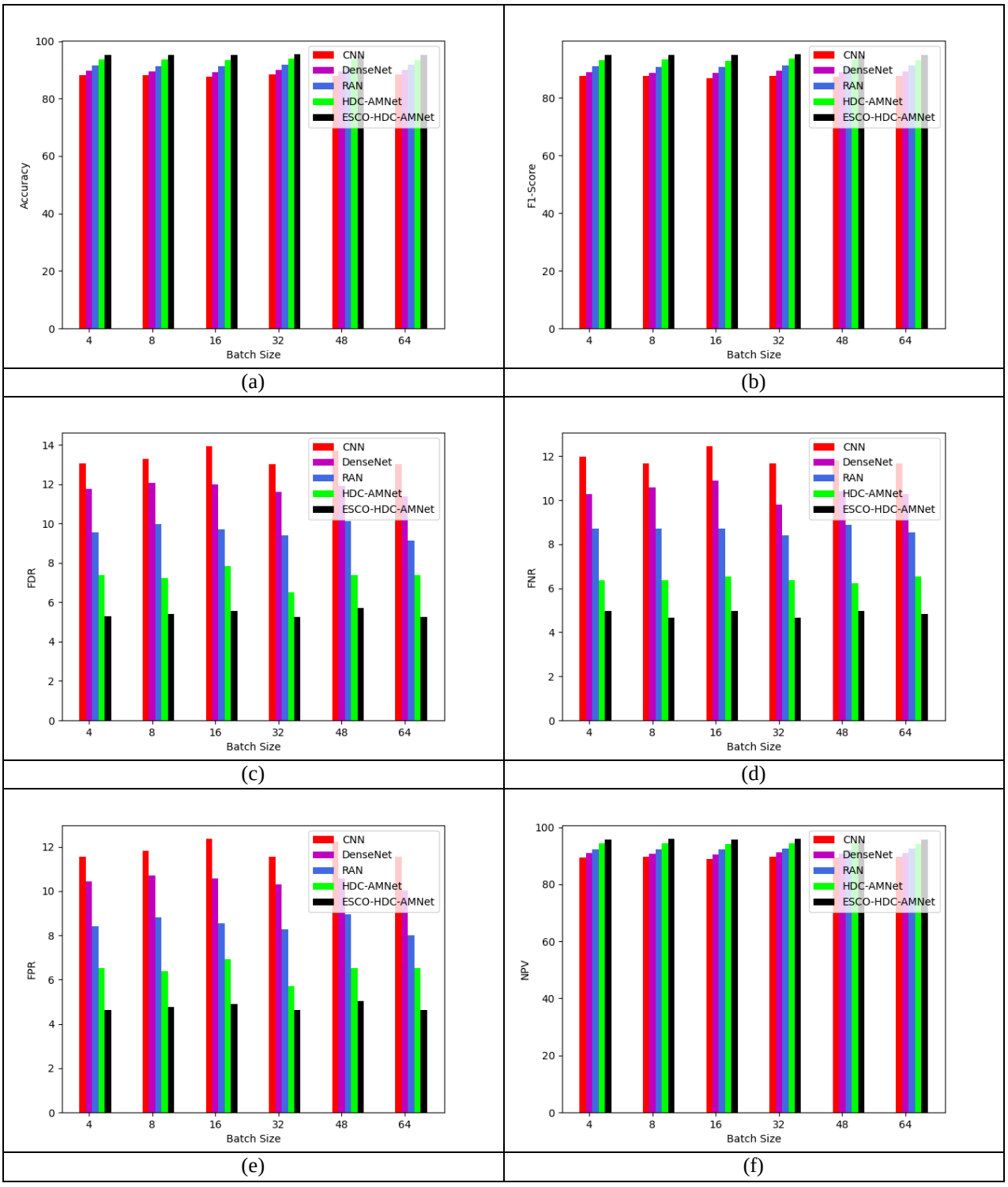
Accuracy
F1-Score
FDR
FNR
FPR
NPV
Batch Size
CNN
DenseNet
RAN
HDC-AMNet
ESCO-HDC-AMNet
(a)
(b)
(c)
(d)
(e)
(f)

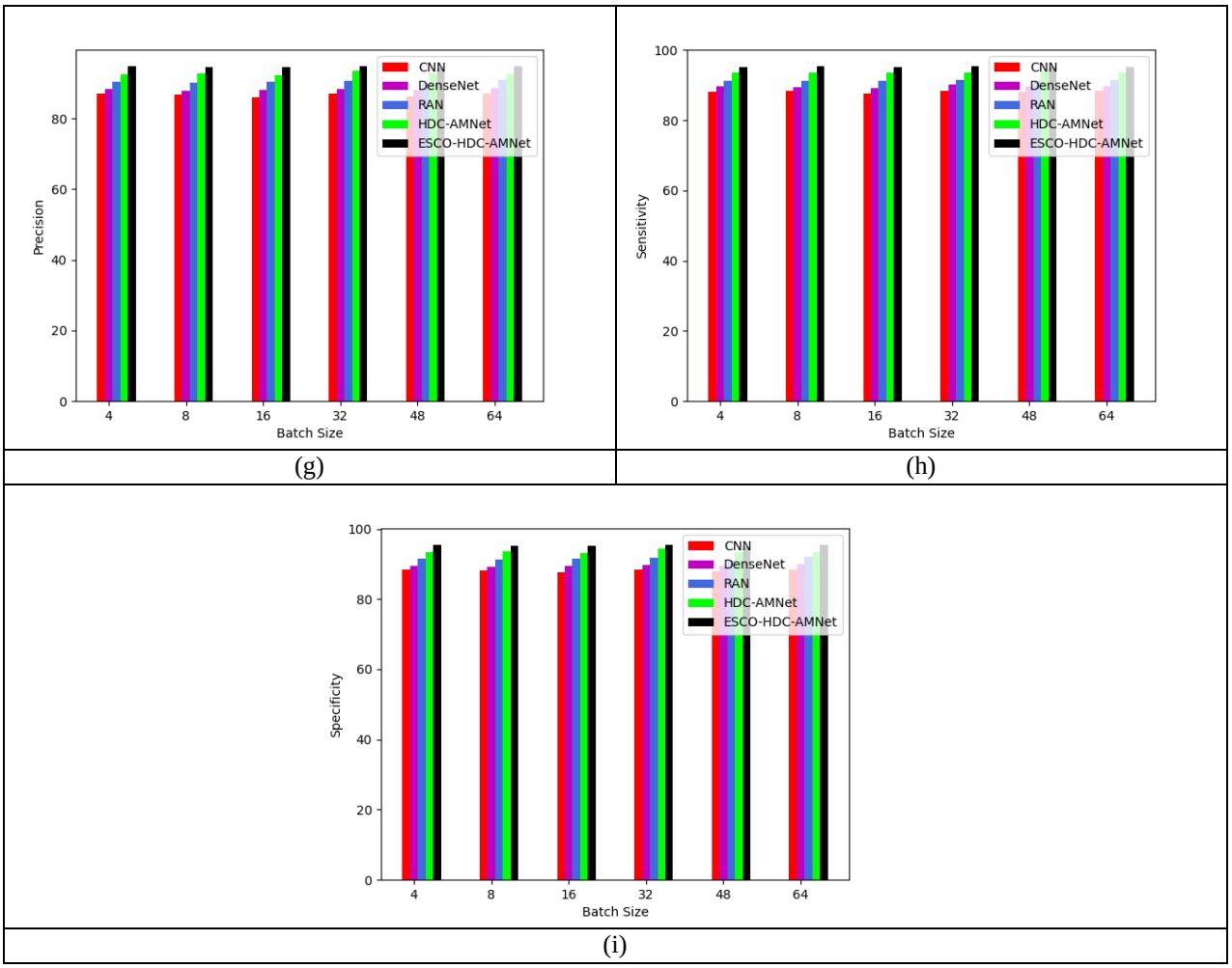

(g) (h)

(i)

Figure 19 Performance evaluation of designed MS classification technique over existing techniques using T2 images concerning "(a) Accuracy, (b) F1-score, (c) FDR, (d) FNR, (e) FPR, (f) NPV, (g) Precision, (h) Sensitivity, and (i) Selectivity"

K. Overall comparative evaluation of recommended MS classification over diverse algorithms and classifiers

The overall comparative estimation of the suggested MS classification technique is carried out using three kinds of images such as FLAIR, T1, and T2 over traditional algorithms and classifiers. The overall comparative estimation is shown in Table III and Table IV over traditional algorithms and mechanisms. When considering T2 images in Table IV, the designed MS classification technique's FNR is decreased by 12.8% of CNN, 10.6% of DenseNet, 6.8% of RAN, and 2.8% of ADC-AMNet accordingly. The results explained that the implemented task provided more effective outcomes for other FLAIR and T1 images. Therefore, it is proved that the designed MS classification task has better efficacy than the other models.

TABLE III. **OVERALL COMPARATIVE ANALYSIS OF DEVELOPED MS CLASSIFICATION TECHNIQUE OVER MULTIPLE ALGORITHMS USING FLAIR, T1, AND T2 IMAGES**

TERMS	DOA-HDC-AMNet [32]	RSA-HDC-AMNet [33]	TFMO-HDC-AMNet [34]	SCO-HDC-AMNet [26]	ESCO-HDC-AMNet
"FLAIR"					
"Accuracy"	87.31909028	90.97174363	89.31771192	92.7636113	94.76223294
"Sensitivity"	87.16645489	90.97839898	89.07242694	92.63024142	94.79034307
"Specificity"	87.5	90.96385542	89.60843373	92.92168675	94.72891566
"Precision"	89.20676203	92.26804124	91.03896104	93.94329897	95.51856594
"FPR"	12.5	9.036144578	10.39156627	7.078313253	5.271084337

"FNR"	12.83354511	9.021601017	10.92757306	7.369758577	5.209656925
"NPV"	85.19061584	89.48148148	87.37151248	91.40740741	93.88059701
"FDR"	10.79323797	7.731958763	8.961038961	6.056701031	4.481434059
"F1-Score"	88.1748072	91.61868202	90.04495825	93.28214971	95.15306122
"MCC"	74.53179495	81.84583183	78.54555075	85.45125804	89.45919069
"T1"					
"Accuracy"	87.33431517	91.089838	89.61708395	92.78350515	95.87628866
"Sensitivity"	87.5	91.40625	88.54166667	92.70833333	95.83333333
"Specificity"	87.26899384	90.9650924	90.04106776	92.81314168	95.89322382
"Precision"	73.04347826	79.95444191	77.80320366	83.56807512	90.19607843
"FPR"	12.73100616	9.034907598	9.958932238	7.186858316	4.106776181
"FNR"	12.5	8.59375	11.45833333	7.291666667	4.166666667
"NPV"	94.65478842	96.40914037	95.22258415	96.99570815	98.31578947
"FDR"	26.95652174	20.04555809	22.19679634	16.43192488	9.803921569
"F1-Score"	79.62085308	85.29769137	82.82582217	87.90123457	92.92929293
"MCC"	71.14584517	79.31059692	75.75332395	83.00562378	90.10487728
"T2"					
"Accuracy"	87.46376812	89.42028986	90.43478261	92.75362319	95
"Sensitivity"	87.55832037	89.58009331	90.51321928	92.84603421	95.02332815
"Specificity"	87.38127544	89.28086839	90.36635007	92.67299864	94.97964722
"Precision"	85.82317073	87.9389313	89.12710567	91.70506912	94.29012346
"FPR"	12.61872456	10.71913161	9.633649932	7.327001357	5.020352782
"FNR"	12.44167963	10.41990669	9.486780715	7.153965785	4.976671851
"NPV"	88.95027624	90.75862069	91.60935351	93.68998628	95.6284153
"FDR"	14.17682927	12.0610687	10.87289433	8.294930876	5.709876543
"F1-Score"	86.68206313	88.75192604	89.81481481	92.27202473	94.65530596
"MCC"	74.8564753	78.77921447	80.80798258	85.45702165	89.96074716

TABLE IV. **OVERALL COMPARATIVE ANALYSIS OF DEVELOPED MS CLASSIFICATION TECHNIQUE OVER MULTIPLE CLASSIFIERS USING FLAIR, T1, AND T2 IMAGES**

TERMS	CNN [38]	DenseNet [39]	RAN [40]	HDC-AMNet [30] [31]	ESCO-HDC-AMNet
"FLAIR"					
"Accuracy"	87.87043418	91.79875948	90.07580979	93.72846313	94.76223294
"Sensitivity"	87.80177891	91.99491741	89.96188056	93.90088945	94.79034307
"Specificity"	87.95180723	91.56626506	90.21084337	93.52409639	94.72891566
"Precision"	89.62386511	92.82051282	91.5912031	94.50127877	95.51856594
"FPR"	12.04819277	8.43373494	9.789156627	6.475903614	5.271084337
"FNR"	12.19822109	8.005082592	10.03811944	6.099110546	5.209656925
"NPV"	85.88235294	90.61102832	88.3480826	92.82511211	93.88059701
"FDR"	10.37613489	7.179487179	8.408796895	5.498721228	4.481434059
"F1-Score"	88.70346598	92.40587109	90.76923077	94.20012747	95.15306122
"MCC"	75.62980096	83.49633664	80.05591973	87.37567445	89.45919069
"T1"					
"Accuracy"	87.92341679	91.1634757	89.32253314	93.59351988	95.87628866
"Sensitivity"	87.5	91.40625	89.84375	93.48958333	95.83333333
"Specificity"	88.09034908	91.06776181	89.11704312	93.63449692	95.89322382
"Precision"	74.33628319	80.1369863	76.49667406	85.27315914	90.19607843
"FPR"	11.90965092	8.932238193	10.88295688	6.36550308	4.106776181
"FNR"	12.5	8.59375	10.15625	6.510416667	4.166666667
"NPV"	94.70198675	96.41304348	95.70011025	97.33191035	98.31578947
"FDR"	25.66371681	19.8630137	23.50332594	14.72684086	9.803921569
"F1-Score"	80.38277512	85.40145985	82.63473054	89.19254658	92.92929293

"MCC"	72.24006454	79.45683142	75.50308173	84.83449006	90.10487728
"T2"					
"Accuracy"	88.62318841	89.63768116	91.30434783	93.62318841	95
"Sensitivity"	88.64696734	89.73561431	91.60186625	93.62363919	95.02332815
"Specificity"	88.60244233	89.55223881	91.04477612	93.62279512	94.97964722
"Precision"	87.1559633	88.22629969	89.92366412	92.75808937	94.29012346
"FPR"	11.39755767	10.44776119	8.955223881	6.377204885	5.020352782
"FNR"	11.35303266	10.26438569	8.398133748	6.376360809	4.976671851
"NPV"	89.94490358	90.90909091	92.55172414	94.39124487	95.6284153
"FDR"	12.8440367	11.77370031	10.07633588	7.241910632	5.709876543
"F1-Score"	87.89514264	88.97455667	90.7550077	93.18885449	94.65530596
"MCC"	77.17510254	79.21158518	82.56097091	87.19787076	89.96074716

VII. CONCLUSION

This work has explored deep learning methodologies for effectively classifying the MS. At first, the necessary images were attained from the standard dataset and these images were transferred to the segmentation stage. In this, the recommended TUnet++-MNetv3 technique, which was the integration of transformer Unet++ and MobileNetv3 was employed for segmenting the image abnormalities. Further, the segmented images were fed into the next module, where the MS lesions were classified with the assistance of the suggested HDC-AMNet technique. Here, techniques such as hybrid dilated convolution and the MobileNet were integrated for classifying the MS. Moreover, the ESCO algorithm was adopted in this classification phase to improve the effectiveness of the process. Finally, experiments were conducted for the implemented framework over other related techniques. The overall accuracy of the designed MS classification process was enhanced by 7.86% of DOA-HDC-AMNet, 3.99% of RSA-HDC-AMNet, 5.75% of TFMO-HDC-AMNet, and 2.11% of SCO-HDC-AMNet appropriately when considering the FLAIR images. Hence, it has been ensured that the developed classification system of MS achieved more promising outcomes than the other related techniques. In the future, the implemented MS classification framework will be improved to process various image modalities with good accuracy.

ACKNOWLEDGMENT

The work was supported by the National Key R&D Program of China (No.2018AAA0102100); the National Natural Science Foundation of China (Nos.U22A2034, 62177047); the Key Research and Development Program of Hunan Province (No.2022SK2054); Central South University Research Programme of Advanced Interdisciplinary Studies (No.2023QYJC020).

REFERENCES

[1] Ye, Z., George, A., Wu, A.T., Niu, X., Lin, J., Adusumilli, G., Naismith, R.T., Cross, A.H., Sun, P., and Song, S.K., "Deep learning with diffusion basis spectrum imaging for classification of multiple sclerosis lesions", Annals of clinical and translational neurology, vol.7, pp.695-706, 2020.

[2] Wang, S.H. and Zhang, Y.D., "DenseNet-201-based deep neural network with composite learning factor and precomputation for multiple sclerosis classification", ACM Transactions on Multimedia Computing, Communications, and Applications (TOMM), vol.16, pp.1-19, 2020.

[3] Soltani, A. and Nasri, S., "Improved algorithm for multiple sclerosis diagnosis in MRI using convolutional neural network", IET Image Processing, vol.14, pp.4507-4512, 2020.

[4] Garcia-Martin, E., Ortiz, M., Boquete, L., Sánchez-Morla, E.M., Barea, R., Cavaliere, C., Vilades, E., Orduna, E. and Rodrigo, M.J., "Early diagnosis of multiple sclerosis by OCT analysis using Cohen's d method and a neural network as classifier", Computers in Biology and Medicine, vol.129, no.104165, 2021.

[5] Cetin, O., Seymen, V. and Sakoglu, U., "Multiple sclerosis lesion detection in multimodal MRI using simple clustering-based segmentation and classification", Informatics in Medicine Unlocked, vol.20, no.100409, 2020.

[6] Buyukturkoglu, K., Zeng, D., Bharadwaj, S., Tozlu, C., Mormina, E., Igwe, K.C., Lee, S., Habeck, C., Brickman, A.M., Riley, C.S. and De Jager, P.L., "Classifying multiple sclerosis patients based on SDMT performance using machine learning", Multiple Sclerosis Journal, vol.27, pp.107-116, 2021.

[7] Iswisi, A.F., Karan, O. and Rahebi, J., "Diagnosis of multiple sclerosis disease in brain magnetic resonance imaging based on the Harris Hawks optimization algorithm", BioMed Research International, 2021.

[8] Afzal, H.M., Luo, S., Ramadan, S., Lechner-Scott, J., Amin, M.R., Li, J. and Afzal, M.K., "Automatic and Robust Segmentation of Multiple Sclerosis Lesions with Convolutional Neural Networks", Computers, Materials & Continua, vol.66, 2021.

[9] Mani, A., Santini, T., Puppala, R., Dahl, M., Venkatesh, S., Walker, E., DeHaven, M., Isitan, C., Ibrahim, T.S., Wang, L., and Zhang, T., "Applying deep learning to accelerated clinical brain magnetic resonance imaging for multiple sclerosis", Frontiers in Neurology, vol.12, no..685276, 2021.

[10] Roca, P., Attye, A., Colas, L., Tucholka, A., Rubini, P., Cackowski, S., Ding, J., Budzik, J.F., Renard, F., Doyle, S. and Barbier, E.L., "Artificial intelligence to predict clinical disability in patients with multiple sclerosis using FLAIR MRI", Diagnostic and Interventional Imaging, vol.101, pp.795-802, 2020.

[11] Salem, M., Valverde, S., Cabezas, M., Pareto, D., Oliver, A., Salvi, J., Rovira, À. and Lladó, X., "A fully convolutional neural network for new T2-w lesion detection in multiple sclerosis", NeuroImage: Clinical, vol.25, no.102149, 2020.

[12] Ansari, S.U., Javed, K., Qaisar, S.M., Jillani, R. and Haider, U., "Multiple sclerosis lesion segmentation in brain MRI using inception modules embedded in a convolutional neural network", Journal of Healthcare Engineering, pp.1-10, 2021.

[13] Rocca, M.A., Anzalone, N., Storelli, L., Del Poggio, A., Cacciaguerra, L., Manfredi, A.A., Meani, A. and Filippi, M., "Deep learning on conventional magnetic resonance imaging improves the diagnosis of multiple sclerosis mimics", Investigative Radiology, vol.56, pp.252-260, 2021.

[14] Montolío, A., Martín-Gallego, A., Cegoñino, J., Orduna, E., Vilades, E., Garcia-Martin, E. and Del Palomar, A.P., "Machine learning in diagnosis and disability prediction of multiple sclerosis using optical coherence tomography", Computers in Biology and Medicine, vol.133, no.104416, 2021.

[15] P. Schwab and W. Karlen, "A Deep Learning Approach to Diagnosing Multiple Sclerosis from Smartphone Data," IEEE Journal of Biomedical and Health Informatics, vol. 25, no. 4, pp. 1284-1291, April 2021.

[16] Narayana, P.A., Coronado, I., Sujit, S.J., Wolinsky, J.S., Lublin, F.D. and Gabr, R.E., "Deep learning for predicting enhancing lesions in multiple sclerosis from non-contrast MRI", Radiology, vol.294, pp.398-404, 2020.

[17] Storelli, L., Azzimonti, M., Gueye, M., Vizzino, C., Preziosa, P., Tedeschi, G., De Stefano, N., Pantano, P., Filippi, M. and Rocca, M.A., "A deep learning approach to predicting disease progression in multiple sclerosis using magnetic resonance imaging", Investigative Radiology, vol.57, pp.423-432, 2022.

[18] Gaj, S., Ontaneda, D. and Nakamura, K., "Automatic segmentation of gadolinium-enhancing lesions in multiple sclerosis using deep learning from clinical MRI", PloS one, vol.16, no.e0255939, 2021.

[19] López-Dorado, A., Ortiz, M., Satue, M., Rodrigo, M.J., Barea, R., Sánchez-Morla, E.M., Cavaliere, C., Rodríguez-Ascariz, J.M., Orduna-Hospital, E., Boquete, L. and Garcia-Martin, E., "Early diagnosis of multiple sclerosis using swept-source optical coherence tomography and convolutional neural networks trained with data augmentation", Sensors, vol.22, no.167, 2021.

[20] McKinley, R., Wepfer, R., Aschwanden, F., Grunder, L., Muri, R., Rummel, C., Verma, R., Weisstanner, C., Reyes, M., Salmen, A. and Chan, A., "Simultaneous lesion and brain segmentation in multiple sclerosis using deep neural networks", Scientific reports, vol.11, no.1087, 2021.

[21] Zhang, Y., Hong, D., McClement, D., Oladosu, O., Pridham, G. and Slaney, G., "Grad-CAM helps interpret the deep learning models trained to classify multiple sclerosis types using clinical brain magnetic resonance imaging", Journal of Neuroscience Methods, vol.353, no.109098, 2021.

[22] Finck, T., Li, H., Grundl, L., Eichinger, P., Bussas, M., Mühlau, M., Menze, B. and Wiestler, B., "Deep-learning generated synthetic double inversion recovery images improve multiple sclerosis lesion detection", Investigative Radiology, vol.55, pp.318-323, 2020.

[23] La Rosa, F., Beck, E.S., Maranzano, J., Todea, R.A., van Gelderen, P., de Zwart, J.A., Luciano, N.J., Duyn, J.H., Thiran, J.P., Granziera, C. and Reich, D.S., "Multiple sclerosis cortical lesion detection with deep learning at ultra-high-field MRI", NMR in Biomedicine, vol.35, no.e4730, 2022.

[24] Alijamaat, A., NikravanShalmani, A. and Bayat, P., "Multiple sclerosis identification in brain MRI images using wavelet convolutional neural networks", International Journal of Imaging Systems and Technology, vol.31, pp.778-785, 2021.

[25] McKinley, R., Wepfer, R., Grunder, L., Aschwanden, F., Fischer, T., Friedli, C., Muri, R., Rummel, C., Verma, R., Weisstanner, C. and Wiestler, B., "Automatic detection of lesion load change in Multiple Sclerosis using convolutional neural networks with segmentation confidence", NeuroImage: Clinical, vol.25, no.102104, 2020.

[26] Tareq M. Shami, David Grace, Alister Burr & Paul D. Mitchell, "Single candidate optimizer: a novel optimization algorithm," Evolutionary Intelligence, 2022.

[27] Yan, H., Deng, B., Li, X. and Qiu, X., "TENER: adapting transformer encoder for named entity recognition", arXiv preprint, 2019.

[28] Nemani, P. and Vollala, S., "Medical image segmentation using levit-unet++: A case study on gi tract data", IEEE, pp. 7-13, 2022.

[29] Alsenan, A., Ben Youssef, B. and Alhichri, H., "Mobileunetv3—a combined unit and mobilenetv3 architecture for spinal cord gray matter segmentation", Electronics, vol.11, no.2388, 2022.

[30] Li, C., Qiu, Z., Cao, X., Chen, Z., Gao, H., and Hua, Z., "Hybrid dilated convolution with multi-scale residual fusion network for hyperspectral image classification", Micromachines, vol.12, no.545, 2021.

[31] Rogelio, J., Dadios, E., Bandala, A., Becerra, R.R. and Sybingco, E., "Alignment control using visual servoing and mobile net single-shot multi-box detection (SSD): A review", International Journal of Advances in Intelligent Informatics, vol.8, pp.97-114, 2022.

[32] Amit Kumar Bairwa, Sandeep Joshi, and Dilbag Singh, "Dingo Optimizer: A Nature-Inspired Metaheuristic Approach for Engineering Problems, " Mathematical Problems in Engineering, 2021.

[33] Z. Elgamal, A. Q. M. Sabri, M. Tubishat, D. Tbaishat, S. N. Makhadmeh, and O. A. Alomari, "Improved Reptile Search Optimization Algorithm Using Chaotic Map and Simulated Annealing for Feature Selection in Medical Field," IEEE Access, vol. 10, pp. 51428-51446, 2022.

[34] Andrei V Panteleev and Anna A. Kolessa, "Application of the Tomtit Flock Metaheuristic Optimization Algorithm to the Optimal Discrete Time Deterministic Dynamical Control Problem," Algorithms, 2022.

[35] Y. Wang, L. Gu, T. Jiang, and F. Gao, "MDE-UNet: A Multitask Deformable UNet Combined Enhancement Network for Farmland Boundary Segmentation," IEEE Geoscience and Remote Sensing Letters, vol. 20, pp. 1-5, 2023.

[36] S. Chen, F. Lei, Z. Zang, and M. Zhang, "Forest Mapping Using a VGG16-UNet++& Stacking Model Based on Google Earth Engine in the Urban Area," IEEE Geoscience and Remote Sensing Letters, vol. 20, pp. 1-5, 2023.

[37] Jieneng Chen, Yongyi Lu, Qihang Yu, Xiangde Luo, Ehsan Adeli, Yan Wang, Le Lu, Alan. Yuille, and Yuyin Zhou, "TransUNet: Transformers Make Strong Encoders for Medical Image Segmentation," Computer Vision and Pattern Recognition, 8 Feb 2021.

[38] S. Montaha, S. Azam, A. K. M. R. H. Rafid, M. Z. Hasan, A. Karim and A. Islam, "TimeDistributed-CNN-LSTM: A Hybrid Approach Combining CNN and LSTM to Classify Brain Lesions on 3D MRI Scans Performing Ablation Study," IEEE Access, vol. 10, pp. 60039-60059, 2022.

[39] K. Zhang, Y. Guo, X. Wang, J. Yuan and Q. Ding, "Multiple Feature Reweight DenseNet for Image Classification," IEEE Access, vol. 7, pp. 9872-9880, 2019.

[40] R. Liu, B. Cui, X. Fang, B. Guo, Y. Ma, and J. An, "Super-Resolution of GF-1 Multispectral Wide Field of View Images via a Very Deep Residual Coordinate Attention Network," IEEE Geoscience and Remote Sensing Letters, vol. 19, pp. 1-5, 2022.